AD-A183 468 COLLOIDAL DYNAMICS SIMULATIONS OF RHEOLOGY AND STABILITY OF CONCENTRATED ... (U) PHYSICAL SCIENCES INC ANDOVER MA ... WILEMSKI 10 APR 87 PSI-3009/TR-668 1/1

UNCLASSIFIED AFOSR-TR-87-0841 F49620-86-C-0072 F/G 21/4 NL

[redacted]

END
DATE FILMED
8 87

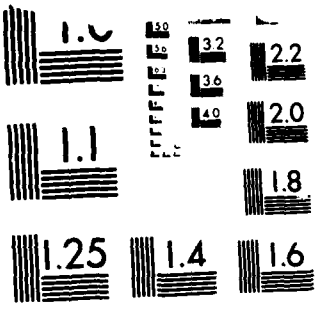

Report PSI-2009/TR-666

COLLOIDAL DYNAMICS SIMULATIONS OF RHEOLOGY AND STABILITY OF CONCENTRATED FUEL SLURRIES

Gerald Wilemski
Physical Sciences Inc.
Research Park, P.O. Box 3100
Andover, MA 01810

10 April 1987

Phase I SBIR Final Report
Contract No. F49620-86-C-0072

Prepared for
AIR FORCE OFFICE OF SCIENTIFIC RESEARCH
Bolling Air Force Base, DC 20332-6449

UNCLASSIFIED
SECURITY CLASSIFICATION OF THIS PAGE

REPORT DOCUMENTATION PAGE

1a. REPORT SECURITY CLASSIFICATION Unclassified	1b. RESTRICTIVE MARKINGS
2a. SECURITY CLASSIFICATION AUTHORITY N/A since Unclassified	3. DISTRIBUTION/AVAILABILITY OF REPORT Unclassified/Unlimited Distribution
2b. DECLASSIFICATION/DOWNGRADING SCHEDULE N/A since Unclassified	
4. PERFORMING ORGANIZATION REPORT NUMBER(S) PSI-2009/TR-666	5. MONITORING ORGANIZATION REPORT NUMBER(S) AFOSR-TR-87-0841
6a. NAME OF PERFORMING ORGANIZATION Physical Sciences Inc. — 6b. OFFICE SYMBOL (If applicable)	7a. NAME OF MONITORING ORGANIZATION Air Force Office of Scientific Research
6c. ADDRESS (City, State and ZIP Code) Research Park, P.O. Box 3100 Andover, MA 01810	7b. ADDRESS (City, State and ZIP Code) Bolling Air Force Base, DC 20332-6449 BC 1410
8a. NAME OF FUNDING/SPONSORING ORGANIZATION Air Force Office of Scientific Research — 8b. OFFICE SYMBOL (If applicable) AFOSR/NA	9. PROCUREMENT INSTRUMENT IDENTIFICATION NUMBER F49620-86-C-0072
8c. ADDRESS (City, State and ZIP Code) same as 7b	10. SOURCE OF FUNDING NOS. PROGRAM ELEMENT NO. 65502F — PROJECT NO. 3005 — TASK NO. A1 — WORK UNIT NO.
11. TITLE (Include Security Classification) Colloidal Dynamics of Rheology and Stability of Concentrated Fuel Slurries	
12. PERSONAL AUTHOR(S) Gerald Wilemski	
13a. TYPE OF REPORT Final Report — 13b. TIME COVERED FROM 860815 TO 870415	14. DATE OF REPORT (Yr., Mo., Day) 870410 — 15. PAGE COUNT 57
16. SUPPLEMENTARY NOTATION	
17. COSATI CODES: FIELD / GROUP / SUB. GR.	18. SUBJECT TERMS (Continue on reverse if necessary and identify by block number) Colloidal dynamics, Rheology, Fuel slurries, Computer simulation

19. ABSTRACT (Continue on reverse if necessary and identify by block number)

This report presents the results of a Phase I SBIR project to calculate properties of concentrated colloidal suspensions using computer simulation methods. Equilibrium and non-equilibrium Brownian dynamics (NEBD) simulations were performed for concentrated aqueous and nonaqueous colloidal suspensions. These are the first calculations of suspension shear viscosity based on NEBD simulations. Stability estimates were also made for sterically stabilized nonaqueous suspensions. The NEBD calculations provide quantitative evidence for the disturbance of the equilibrium structure of the dispersions by shearing. Shear viscosities have been calculated as a function of shear rate and particle volume fraction. Good agreement was obtained with experimental viscosities for comparable systems. The simulation results are sensitive to the type, strength and range of the potential interactions used to describe the dispersion. These results demonstrate that the NEBD technique is capable of describing the essential features of sheared suspension behavior. They also establish the feasibility and desirability of using NEBD simulation methods as a predictive engineering tool for the design of slurries.

20. DISTRIBUTION/AVAILABILITY OF ABSTRACT UNCLASSIFIED/UNLIMITED ☒ SAME AS RPT ☐ OTIC USERS ☐	21. ABSTRACT SECURITY CLASSIFICATION Unclassified
22a. NAME OF RESPONSIBLE INDIVIDUAL Julian Tishkoff	22b. TELEPHONE NUMBER (Include Area Code) (202) 767-4935 — 22c. OFFICE SYMBOL AFOSR/NA

DD FORM 1473, 83 APR — EDITION OF 1 JAN 73 IS OBSOLETE

UNCLASSIFIED
SECURITY CLASSIFICATION OF THIS PAGE

CERTIFICATION OF TECHNICAL DATA CONFORMITY

(OCTOBER 1985) (DOD FAR 52.227-7036)

The Contractor, Physical Sciences Inc. (PSI), hereby certifies that, to the best of its knowledge and belief, the technical data delivered herewith under Contract No. F49620-86-C-0072 is complete, accurate, and complies with all requirements of the contract.

4/13/87
Date

Michael L. Finson, Executive Vice President

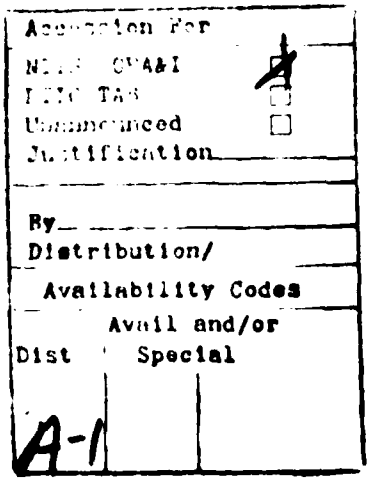

EXECUTIVE SUMMARY

The general aim of this Phase I SBIR project was to extend and refine existing computer simulation capabilities in order to compute equilibrium and nonequilibrium properties of concentrated colloidal suspensions. The immediate application of this work is to guide improvements in the characteristics of nonaqueous colloidal fuel slurries that are currently being developed by the Air Force for use as propellants.

Equilibrium and nonequilibrium Brownian dynamics simulation techniques were employed in this work. The simulations include the effects of interparticle forces, Brownian motion and shear flow on the motion of particles. Hydrodynamic interactions were neglected in accordance with the Phase I work plan.

Equilibrium and nonequilibrium Brownian dynamics (NEBD) simulations were performed for concentrated aqueous and nonaqueous colloidal suspensions. These are the first NEBD simulations in which the shear viscosities of suspensions have been calculated. Stability estimates were also made for sterically stabilized nonaqueous suspensions. These results can be understood in terms of the changes occurring in the repulsive steric potential and attractive van der Waals potential as the adsorbed polymer concentration and Hamaker constant are changed.

These calculations provide quantitative evidence for the disturbance of the equilibrium structure of the dispersions by shearing. Shear viscosities of suspensions have been calculated as a function of shear rate and particle volume fraction. Good agreement was obtained with experimental viscosities for comparable systems. The simulation results are sensitive to the type, strength and range of the potential interactions used to describe the dispersion. Thee overall conclusion of this Phase I study is that the NEBD technique is capable of describing the essential features of sheared suspension behavior. These Phase I results establish the feasibility and desirability of using NEBD simulation methods as a predictive engineering tool for the design of slurries.

ACKNOWLEDGEMENTS

I thank Dr. R. Cook of Lawrence Livermore National Laboratory and Dr. A. Gelb of Physical Sciences Inc. for their valuable comments and suggestions.

CONTENTS

LIST OF ILLUSTRATIONS

LIST OF ILLUSTRATIONS (Cont.)

1. INTRODUCTION

The general aim of this Phase I SBIR project was to extend and refine existing computer simulation capabilities in order to compute equilibrium and nonequilibrium properties of concentrated colloidal suspensions. Nonaqueous colloidal fuel slurries are currently being developed by the Air Force for use as propellants. The primary goal of this research was to perform, for the first time, nonequilibrium Brownian dynamics simulations of sheared concentrated suspensions in order to calculate the shear viscosity of these systems. This has been accomplished. By comparing the calculated viscosities and their dependence on particle volume fraction and shear rate with observed properties of real systems, the feasibility of this approach as a slurry design tool has been established. Sample calculations of suspension stability using classical coagulation theory have also been done to illustrate the interplay of repulsive and attractive forces in stabilizing suspensions.

Because of the many different types of forces and interactions between colloidal particles, these suspensions display complicated behavior, and current theoretical understanding of them is limited.[1-5] Exact theories do not exist except for a few idealized, limiting cases. Approximate theories are invariably forced to omit or oversimplify one or more of the important classes of particle interactions for the sake of mathematical tractability. Computer simulation techniques, on the other hand, are capable of treating more-or-less exactly all forms of particle interactions, at the expense, admittedly, of ever increasing computational effort with growth in the size of the system or number of effects treated. However, modern computers are sufficiently fast to overcome these limitations for many systems of practical interest. Thus, these methods are a promising means for obtaining insight into the microscopic reasons underlying the observed behavior of concentrated suspensions.

Equilibrium and nonequilibrium simulations of concentrated aqueous and nonaqueous suspensions were performed. Aqueous systems were studied for two reasons. First, results of prior equilibrium simulations of aqueous systems

have been published and are available for comparison. Second, experimental shear viscosity data on well-characterized suspensions cover a somewhat broader range of conditions for aqueous systems, which have been studied more extensively than nonaqueous systems. Equilibrium simulations of strongly interacting dilute systems were also performed under previous PSI in-house support. The results of these comparisons are described in Appendix A as additional background material.

It should be noted that these are the first nonequilibrium Brownian dynamics (NEBD) simulations in which the shear viscosity of a suspension has been calculated. Several different interparticle force laws were studied, although hydrodynamic interactions were neglected in accordance with the limited Phase I work plan. Previous BD simulations with shear and hydrodynamic interactions,[6] have been concerned with the dynamics of coagulation and deflocculation of isolated pairs of particles. Nonequilibrium Stokesian dynamics simulations were developed by Bossis and Brady[7] to treat suspensions of particles large enough that Brownian motion of the particles can legitimately be neglected. This method includes hydrodynamic interactions but has so far only been used to calculate the shear viscosity of two dimensional suspensions.[7,8] Many nonequilibrium molecular dynamics (NEMD) simulations have been performed to compute the shear viscosity of molecular fluids.[9-12] Because of the vast differences in the size and time scales governing molecular and colloidal particle motion, the NEMD simulations must be performed at extremely high shear rates, exceeding by many orders of magnitude values that can be attained experimentally. Although NEMD techniques are an extremely important development in computational statistical mechanics, they are incapable of treating many inherently colloidal phenomena such as viscous damping of particle motion, hydrodynamic interaction between particles or Brownian motion. Thus, NEMD simulations can provide only some qualitative insights into the rheology of particulate suspensions.

Before describing the results of the nonequilibrium simulations, the theoretical background underlying the computational method is presented in Section 2. Following this, the interparticle pair potentials used in the simulations are discussed in Section 3. As noted, simulations were performed

with pair potentials appropriate for aqueous as well as nonaqueous dispersions. The results of the equilibrium and nonequilibrium simulations of concentrated dispersions are then presented and discussed in Section 4. The stability ratio for nonaqueous sytems is also discussed. Appendix A contains the results of the equilibrium simulations of dilute, but strongly interacting aqueous dispersions.

2. THEORETICAL BACKGROUND

2.1 GENERAL CONSIDERATIONS

The Brownian dynamics (BD) simulation technique is employed in this work. This method is an outgrowth of the molecular dynamics (MD) simulation techniques that are now a well established part of the methodology of modern statistical mechanics.[13] The MD method involves numerically solving Newton's equations of motion for all N particles in the system. It is a deterministic, rather than a stochastic, technique. By keeping track of all the particles' trajectories, a representative sampling of phase space is generated, and averages of system properties can be calculated. Both dynamic and static system properties can be treated. The method is limited to relatively small numbers of particles, generally less than a thousand, because of computer speed and size limitations.

Because of the vast difference in size and mass between a typical suspended particle and a molecule of the suspending fluid, the time and length scales for simultaneous motion of molecules and particles cover too many orders of magnitude to be directly treated by MD techniques. To overcome this problem, BD techniques[14-18] have been developed to simulate suspensions. In the BD technique, the suspending fluid is treated as a hydrodynamic and dielectric continuum and the motions of the suspended particles are described by Langevin equations. Langevin equations are stochastic differential equations that play the role of Newton's equations in the molecular dynamics simulation. The Langevin equations describe the motions of the particles subject to the action of interparticle and external forces, frictional forces arising from solvent drag, and random Brownian motion forces. The Brownian forces are assumed to act on a time scale that is much shorter than that required to produce even a modest change in the particle's location or velocity, and they must be treated statistically, as described below, to account for their cumulative efffect on the motion of the colloidal particle. From the solution of the Langevin equations for the interacting many particle system, positions of the N colloidal particles can be computed as a function of time. From this

information, one can calculate fundamental quantities of interest such as mean square particle displacements, pair distributuion functions, and transport properties such as the self-diffusion coefficient and the shear viscosity.

2.2 PARTICLE INTERACTIONS

Solution of the equations of motion for individual particle displacements requires knowledge of the interparticle forces and interactions affecting each particle. These may be broken down into three groups.

First, there are random Langevin forces responsible for the Brownian motion of the particles. Langevin forces arise from the (small) fluctuations in the (very large) number of collisions experienced by different areas of the large particle with the much smaller molecules of the suspending fluid.

The second class of forces consists of the "direct" interparticle forces. These include: (1) repulsive (or excluded volume) forces due to the finite size and relatively small deformability of the particles, (2) short-ranged oscillatory forces between closely spaced particles due to fluid structure and packing,[19,20] (3) forces due to absorbed polymer molecules which, under conditions giving rise to net repulsion, result in so-called steric stabilization,[21] (4) attractive London-van der Waals forces, and (5) repulsive forces due to the overlap of electrical double layers surrounding similar particles. The latter two forces form the basis for the classical DLVO theory of colloid stability.[22,23] The attractive van der Waals force between large suspended particles at small separations d varies as d^{-2},[24] considerably different from the short ranged d^{-7} dependence typical of molecular interactions. Electrical double layer repulsions (or attractions for dissimilar particles under the right conditions) result from overlap of the diffuse clouds of counter ions surrounding a charged suspension particle. For situations of weak overlap the interaction force for large particles varies exponentially with d; with the length scale set by the familar Debye parameter[25] (or inverse screening length), κ. In non-aqueous media, electrical double layer interactions are generally unimportant.

The third group of interactions consists of hydrodynamic interactions between particles. The term refers to the interaction between particles due to the velocity fields set up in the fluid by the moving particles. These velocity disturbances propagate through the fluid, perturbing the motion of nearby particles.

Hydrodynamic interactions are neglected in this early developmental work, and will only be cursorily treated in describing the algorithm for colloidal particle motion.

2.3 LANGEVIN EQUATIONS

The Langevin equation governing the motion of colloidal particle i of mass m_i can be written[6] as

$$m_i \frac{d\underset{\sim}{v}_i}{dt} = -\sum_j \underset{\sim}{\zeta}_{ij} \cdot \left(\underset{\sim}{v}_j - \underset{\sim}{u}_j + \underset{\sim}{S}_j : \underset{\sim}{E}\right) + \underset{\sim}{F}_i + \underset{\sim}{L}_i \qquad (1)$$

where $\underset{\sim}{v}_i$ is the particle velocity, $\underset{\sim}{F}_i$ is the total force (direct contact plus external, if present) on the particle, $\underset{\sim}{L}_i$ is the random Langevin force responsible for the particle's Brownian motion, $\underset{\sim}{u}_i$ is the undisturbed fluid velocity at the location of particle i due to an externally imposed flow field. Hydrodynamic interactions between particles are governed by the configuration dependent second rank friction (or resistance) tensor $\underset{\sim}{\zeta}$ and the configuration dependent third rank shear tensor $\underset{\sim}{S}$. The rate of strain tensor $\underset{\sim}{E}$ is given as usual by the expression

$$\underset{\sim}{E} = \frac{1}{2}\left[\underset{\sim}{\nabla u} + \left(\underset{\sim}{\nabla u}\right)^T\right] \quad . \qquad (2)$$

For the case of simple shear flow in the x direction, the unperturbed fluid velocity flow field is given by

$$\underset{\sim}{u}_i = \dot{\gamma}\, y_i\, \underset{\sim}{e}_x \qquad (3)$$

where $\dot{\gamma}$ is the shear rate (s^{-1}) and y_i is the y coordinate of particle i in some Cartesian coordinate system with unit basis vectors ($\underset{\sim}{e}_x$, $\underset{\sim}{e}_y$, $\underset{\sim}{e}_z$).

The first term in Eq. (1) represents the frictional resistance on the particle due to solvent drag, hydrodynamic interactions and convective effects in a sheared suspension. With the neglect of hydrodynamic interactions, the shear tensor vanishes,

$$\underset{\sim}{S}_i = 0 \ , \tag{4}$$

and only the diagonal components of the friction tensor remain,

$$\underset{\sim}{\zeta}_{ij} = \zeta_i \delta_{ij} \underset{\sim}{I} \ . \tag{5}$$

Here, ζ_i, the single particle friction coefficient, is customarily evaluated using Stokes' law,

$$\zeta_i = 6\pi\eta_o a \tag{6}$$

where η_o is the pure fluid viscosity (Pa·s) and a is the radius of the particle. Because of Eqs. (4) and (5), with the neglect of hydrodynamic interactions the Langevin Equations for particle motion simplify considerably to the form

$$m_i \frac{d\underset{\sim}{v}_i}{dt} = -\zeta_i(\underset{\sim}{v}_i - \underset{\sim}{u}_i) + \underset{\sim}{F}_i + \underset{\sim}{L}_i \ . \tag{7}$$

The complicated configuration dependence of $\underset{\sim}{F}_i$ still precludes an exact solution of these equations. In order to proceed with the numerical simulation of particle motion, an algorithm is required for computing the change in position of each particle during a small time step Δt. Heuristic arguments will be used to obtain algorithms without and with shear flow that are special cases of those obtained with more rigor by Ermak and McCammon[17] and Ansell, Dickinson, and Ludvigsen.[6]

Particles undergoing Brownian motion incur significant changes in position only on a time scale that is long compared to the typical time for the particle's instantaneous velocity to become uncorrelated with its value at any earlier time.[26] Velocity fluctuations are rapidly damped by fluid friction, and all of the forces acting on a particle are nearly always in balance. The

velocity relaxation time scale is set by the ratio m_i/ζ_i. Thus for a time interval $\Delta t >> m_i/\zeta_i$, the left hand side of Eq. (7) may be neglected, and the remaining terms may be solved for $\underset{\sim}{v}_i$ to give

$$\underset{\sim}{v}_i = \underset{\sim}{u}_i + \underset{\sim}{F}_i/\zeta_i + \underset{\sim}{L}_i/\zeta_i \quad . \tag{8}$$

Equation (8) is the i'th member of a set of N first order, coupled stochastic differential equations for the positions $\underset{\sim}{r}_i$ of the N colloidal Brownian particles in the suspension. Because $d\underset{\sim}{r}_i/dt = \underset{\sim}{v}_i$, it is apparently a simple matter to solve Eq. (8) for the displacement $\Delta\underset{\sim}{r}$ incurred in a time interval short enough that the total force $\underset{\sim}{F}_i$ acting on the particle remains constant. However, solving a stochastic differential equation is different from solving an ordinary partial differential equation. Given the stipulation that $\Delta t >> m_i/\zeta_i$, the product $\underset{\sim}{L}_i \Delta t$ has no meaning because $\underset{\sim}{L}_i$ varies extremely rapidly and randomly within the interval Δt. A correct integration of Eq. (8) results in the following prescription for $\Delta\underset{\sim}{r}_i$:

$$\Delta\underset{\sim}{r}_i = \left(\underset{\sim}{u}_i + D_i \, \underset{\sim}{F}_i/kT\right)\Delta t + \underset{\sim}{R}_i \tag{9}$$

where the random displacement experienced by the particle in Δt is defined as

$$\underset{\sim}{R}_i = \left(1/\zeta_i\right) \int_t^{t+\Delta t} \underset{\sim}{L}_i \, dt' \tag{10}$$

and the self-diffusion coefficient, D_i, of a particle in a highly dilute suspension is given by the Stokes-Einstein expression

$$D_i = kT/\zeta_i = kT/(6\pi\eta_o \, a) \quad . \tag{11}$$

In order to complete the algorithm, the statistical properties of $\underset{\sim}{R}_i$ must be specified. These follow from two basic assumptions of Brownian motion theory regarding the behavior of $\underset{\sim}{L}_i$. First, the average of $\underset{\sim}{L}_i$ over all possible fluctuations is zero,

$$\langle \underset{\sim}{L}_i \rangle_L = \underset{\sim}{0} \quad . \tag{12}$$

Second, values of $\underset{\sim}{L}_i$ at different times are uncorrelated, i.e., $\underset{\sim}{L}_i$ behaves as a white noise source,

$$\langle \underset{\sim}{L}_i(t_1) \cdot \underset{\sim}{L}_i(t_2) \rangle_L = 6\zeta_i kT\, \delta(t_1 - t_2) \quad . \tag{13}$$

The subscript L on the angle brackets in Eq. (12) and (13) indicates an average over all the fluctuating values of $\underset{\sim}{L}_i$. The constants preceding the delta function in Eq. (13) are a consequence of a form of the Fluctuation-Dissipation Theorem. They are there to insure that the long time average value of v_i^2, as determined by exactly solving Eq. (7) without shear ($\underset{\sim}{u}_i$=0), equals $3kT/m_i$, the equipartition value of equilibrium statistical mechanics.

Using the properties shown in Eq. (12) and (13), it is easy to see that

$$\langle \underset{\sim}{R}_i \rangle_L = \underset{\sim}{0} \tag{14}$$

and that

$$\langle R_i^2 \rangle_L = 6D_i \Delta t \quad . \tag{15}$$

Equation (9) may now be written as

$$\Delta \underset{\sim}{r}_i = (\underset{\sim}{u}_i + D_i \underset{\sim}{F}_i/kT)\Delta t + (2D_i \Delta t)^{1/2}\, \underset{\sim}{Q}_i \tag{16}$$

where the components of $\underset{\sim}{Q}_i$ are Gaussian random numbers whose mean and mean square values are zero and one, respectively:

$$\bar{Q}_{xi} = 0, \qquad \overline{Q^2}_{xi} = 1 \quad . \tag{17}$$

Equations (16) and (17) comprise the algorithm for computing the displacements of the colloidal particles. The displacement is seen to result from the superposition of a term linear in Δt, which is due to the shear field (if any) and direct particle interactions, with the Brownian jump term, which varies as the square root of Δt. These equations also give the correct expressions to first order in Δt for the mean and mean square displacements of a diffusing particle in a shear field and subject to interparticle or external forces (but without hydrodynamic interactions):

$$\langle \Delta \underset{\sim}{r}_i \rangle_L = \left(\underset{\sim}{u}_i + D_i \underset{\sim}{F}_i / kT \right) \Delta t \tag{18}$$

$$\langle (\Delta r_i)^2 \rangle_L = 6 D_i \Delta t \quad . \tag{19}$$

The general procedure for carrying out a simulation is as follows. Given a set of particle coordinates at a time t, the forces on each particle are determined, and a set of random numbers $\underset{\sim}{Q}_i$ is generated. The particle positions are then advanced, and the entire process is repeated. The questions of boundary conditions and how to correctly determine the total force on a particle will be dealt with in the following sections.

2.4 PERIODIC BOUNDARY CONDITIONS

In order to insure that a system of N particles (where N is usually less than several hundred) in a cubic cell of volume V (adjusted to give the desired density or volume fraction) will represent a bulk system, the primary cell is surrounded by 26 image cells each containing N particles in the same configuration as the primary cell. Such periodic boundary conditions allow particles to pass through cell walls while preserving constant particle number (and density) in each cell.

The side length ℓ of the cube is determined by specifying the volume fraction ϕ for the suspension in terms of the particle number density and volume,

$$\phi = (N/\ell^3)(\pi d^3/6) \tag{20}$$

where d is the particle diameter.

Consider first the case without shear flow. Because all of the images of a given particle execute the same movements as the particle itself, when the particle passes through one of the cell walls, an appropriate image particle automatically passes through the opposite wall to replace it in the cell. The situation is illustrated in Fig. 1. In practice it is unnecessary to save the coordinates of the image particles because these are easily generated by a

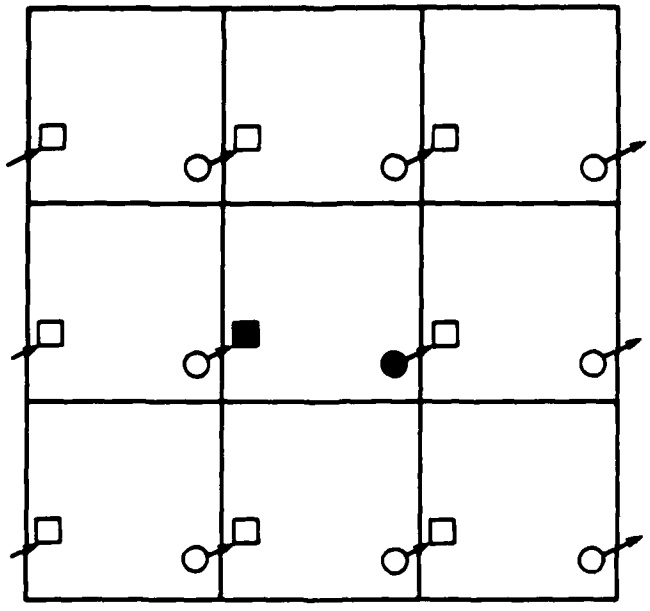

A-5241

Figure 1. Two-dimensional illustration of how periodic boundary conditions simulate an infinite equilibrium system. Circles denote positions before a jump of (exaggerated) magnitude →. Squares indicate positions after the jump. Open symbols represent images surrounding the primary particles (filled symbol).

series of reflections, $x_i+\nu\ell$, $y_i+\nu\ell$, $z_i+\nu\ell$, where ν = -1, 0, and +1. For example, with the coordinate origin at the center of the box, if particle i moves outside the box at $x=\ell/2$, i.e., if $x_i>\ell/2$, it is replaced by an image particle now located at $x_i-\ell$ (within the cube). Similarly, if $x_i<-\ell/2$, then x_i would be replaced by $x_i+\ell$. Similar adjustments are made to y and z coordinates whenever necessary.

In computing the total force on a particle due to interactions with all N-1 remaining particles, the minimum image convention[27] is used. The cut-off distance for particle interactions is taken to be $\ell/2$. Forces between particles farther apart than $\ell/2$ are set equal to zero. This insures that, when $r_{ij}>\ell/2$, particle i will interact with only the nearest image of particle j. The nearest image is located by determining which of the inequalities,

$$-\ell/2<x_{ij}<\ell/2 \tag{21a}$$

$$-\ell/2<y_{ij}<\ell/2 \tag{21b}$$

$$-\ell/2<z_{ij}<\ell/2 \tag{21c}$$

is violated, followed by adjusting the appropriate components of $\underset{\sim}{r}_j$. With a few moments of reflection, it should be clear that Eq. (21) will be satisfied by every pair of particles, provided the nearest image coordinates of j are used whenever appropriate. The situation is illustrated in Fig. 2.

With a shear flow in the x direction, periodic boundary conditions identical to those used without shear are imposed for motion in the x and z directions. Motion in the y direction is subject to the coordinate space version

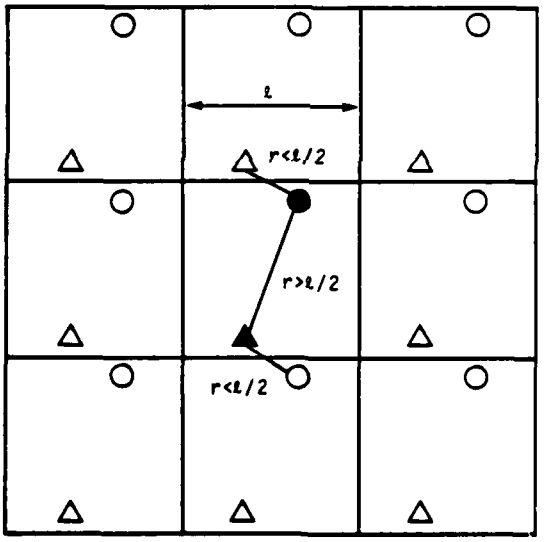

A-5242

Figure 2. Two-dimensional illustration of how particles interact when the minimum image convention is used. The two particles ●, ▲ in the center square are too far apart to interface. The ● particle interacts with the nearest triangular image and the ▲ particle interacts with the nearest circular image.

of the homogeneous shear conditions introduced by Lees and Edwards[28] and Evans.[10] Image particles in the cubes above the plane $y=\ell/2$ and below the plane $y=-\ell/2$ do not simply replicate the motion in the primary cube. If they did, the shear field would exhibit sharp discontinuities at $y=\pm\ell/2$. Because of the homogeneous shear condition, image particles lying above $y=\ell/2$ or below $y=-\ell/2$ suffer added x displacements of magnitude $\ell\dot{\gamma}\Delta t$ in addition to those incurred by the primary particles. This insures that image particles with larger or smaller y values than those of the primary particles experience proportionately larger shear displacements in the appropriate direction.

The result of this procedure is that after n steps the relative x displacement between a particle and its (original) nearest upper and lower images is $n\ell\dot{\gamma}\Delta t$. The particle and these two images lie on a diagonal line in the x-y plane that is rotated through an angle α where $\tan\alpha = n\dot{\gamma}\Delta t$. The situation is illustrated in Fig. 3. When a particle leaves the box at $y=\pm\ell/2$, it is replaced by a particle with new coordinates $(x_i \pm n\ell\dot{\gamma}\Delta t,\ y_i \mp \ell)$; the new x coordinate must also be checked and adjusted, if necessary, to insure that it satisfies the inequality $\ell/2 > x_i > -\ell/2$. When α equals 45°, the additional x displacement between images due to shear vanishes, and the simulation may be continued with n reset to zero.

In computing the total force on particle i, the minimum image convention is again used, but allowance must be made for the relative shear displacement of image particles. When y_{ij} satisfies the inequality

$$-\ell/2 < y_{ij} < \ell/2 \tag{22}$$

the procedure is identical to that in the absence of shear. When $y_{ij} > \ell/2$, x_j must first be changed to $x_j + n\ell\dot{\gamma}\Delta t$ before checking the inequalities in Eq.(21). When $y_{ij} < -\ell/2$, x_j is first changed to $x_j - n\ell\dot{\gamma}\Delta t$ before checking Eq.(21). An illustration is provided in Fig. 4.

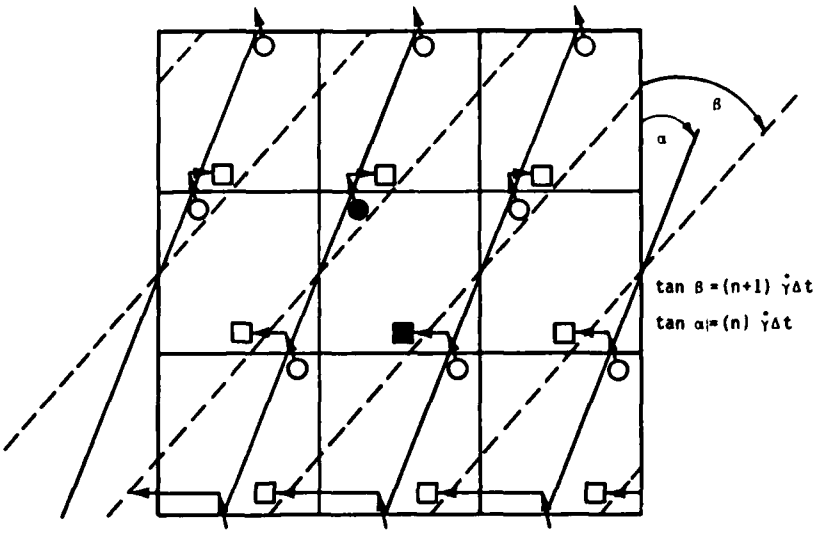

Figure 3. Illustration of how homogeneous shear conditions plus periodic boundary conditions simulate an infinite system being sheared at a shear rate $\dot{\gamma}$. Circles mark positions of particles after n time steps of Δt; squares indicate positions after n+1 steps. The value of $\dot{\gamma}\Delta t$ is exaggerated for clarity. The displacement of particle ● results from the nearly vertical jump due to random and interparticle forces plus the horizontal shear displacement. After n steps, particle ● and its images o lie along the solid diagonal rotated through the angle α. After n+1 steps, particle ■ and its images □ lie along the dashed diagonals that are rotated by the angle β.

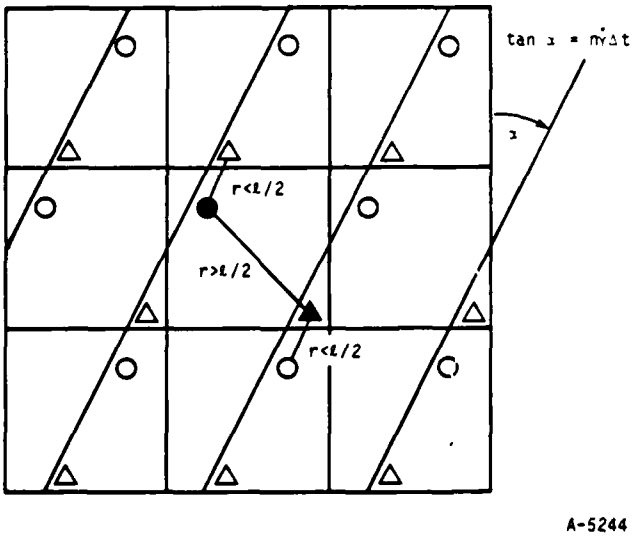

Figure 4. Illustration of how particles interact when homogenous shear conditioning and minimum image convention are used. The two particles ●,▲ in the center square are too far apart to interact. Each interacts with the nearest image of the other, but the effects of shear must be accounted for in locating the images.

2.5 RADIAL DISTRIBUTION FUNCTION

The radial distribution function (or pair correlation function) g(r) provides information about the local distribution of particles in the fluid around any arbitrarily selected particle. Because particles have hard cores and interact with each other via other repulsive and attractive forces, the local distribution may deviate considerably from the simple bulk average. Besides providing insight into the structure of the fluid, g(r) is important for another reason. When particle interactions are assumed to be pairwise additive, all of the (excess) equilibrium thermodynamic properties of the suspension can be obtained solely from g(r). There are a number of simple, equivalent ways of defining g(r). If ρ (=N/V)is the average number density of particles in the suspension, $\rho g(r)$ is the local density at a distance r from any particle. Thus, the quantity $4\pi r^2 \rho g(r)dr$ is the number of particles whose centers lie within a spherical shell of thickness dr at a distance r from the central particle. Finally, $N4\pi r^2 \rho g(r)dr$ is the number of pairs of particles whose center-to-center distance lies between r and r+dr. Because the distances between all pairs of particles are evaluated in determining the total force on each particle, this last definition is most convenient in numerically calculating g(r) during a simulation.

2.6 SELF-DIFFUSION COEFFICIENT

The self-diffusion coefficient for tagged (or tracer) particle motion in suspensions is a good indicator of the effects of concentration, interparticle forces, and hydrodynamic interactions on the ease with which particles move about in the suspension. The time dependent self-diffusion coefficient can be computed from the expression[29,30]

$$D_s = \frac{1}{6}\frac{d}{dt}\langle(\Delta r(t))^2\rangle \qquad (23)$$

where the mean square displacement (m.s.d.) is defined as

$$\langle(\Delta r(t))^2\rangle = \frac{1}{N}\langle \sum_i |\underset{\sim}{r}_i(t) - \underset{\sim}{r}_i(0)|^2 \rangle \qquad (24)$$

and the angle brackets denote an equilibrium ensemble average. The algorithm used to compute the m.s.d. is similar to Van Megen's and Snook's method,[30] which is based on the operation of a hard-wired correlator used in photon correlation spectroscopy experiments.

The m.s.d. is computed at n_s time intervals τ of length $m\Delta t$. The constants m and n_s are chosen to give adequate temporal resolution of the m.s.d. and to insure that the longest sampling time ($n_s\tau$) is less than the time at which the uncertainty in the calculated value of the m.s.d. becomes too large due to statistical fluctuations. Rather than store n_s sets of particle coordinates, as Van Megen and Snook do, a suggestion[31] to store the cumulative displacements is followed. In this way, one avoids having to correct the sequence of coordinates for a particle when that particle passes through any wall of the simulation cube. Failure to correct the coordinates would introduce artificial jumps of length ℓ every time a particle moved through a wall.

The cumulative x, y, and z displacements of the N particles at each of the n_s times are stored in n_s sets of registers. After every m time steps, a new set of initial displacements $\underset{\sim}{\Delta r}(\tau)$ is generated, and the total displacements corresponding to the largest sampling time $n_s\tau$ are discarded. The new displacements are then added to each of the remaining cumulative displacements, thus advancing them by one step of time τ. Each of the cumulative displacements is then shifted to the next storage register, and the new displacements are stored in the first register. In this scheme, the particle trajectories are followed backwards through time (which makes no difference in calculating the m.s.d.), and a new sequence of cumulative displacements is effectively created after every m time steps. From the new sequence of cumulative displacements the squares of the displacements are formed, summed, and added to the existing sums for each time. Ultimately, these sums are averaged over the total number of starting times for which a sequence of displacements was generated.

2.7 SHEAR VISCOSITY

From the nonequilibrium simulations, the shear viscosity coefficient η can be obtained by dividing the average shear stress σ_{xy} of the suspension by the shear rate:

$$\sigma_{xy} = \eta\dot{\gamma} \quad . \tag{25}$$

With the neglect of hydrodynamic interactions, the average shear stress can be calculated by averaging the particle stress tensor:[8,32,33]

$$\sigma_{xy} = \eta_o \dot{\gamma} + \frac{5}{2}\frac{\phi}{1-\phi}\dot{\gamma} + \frac{1}{V}\left\langle \sum_{i>j} y_{ij} F_{xij} \right\rangle \quad . \tag{26}$$

The first term is the pure fluid contribution, the second arises from the hydrodynamic particle stress in the infinitely dilute limit, and the last term represents the contribution of interparticle forces to the stress. Here, the angle brackets denote an average over the nonequilibrium particle distribution in the sheared suspension. The double sum indicated in Eq. (26) is computed after each time step of the simulation. The values are summed and averaged over the total number of time steps in the simulation.

2.8 INITIAL CONDITIONS

Simulations are generally started with the particles arranged on the sites of a fcc lattice. Typically, five thousand time steps (or more, if needed) are then generated in order to bring the system to equilibrium or to steady-state (with shear). Computation of average system properties then commences. In the equilibrium simulations, satisfactory results can usually be obtained with five to ten thousand steps. For the nonequilibrium simulations much longer runs, of thirty thousand steps or more, are required for averaging the particle stress tensor. If the final coordinates from a prior run under identical or similar conditions are available, the preliminary startup period may be eliminated or significantly reduced.

3. DIRECT INTERPARTICLE FORCES

3.1 PAIRWISE ADDITIVITY

Potential interactions between particles were assumed to be pairwise additive. Thus, the total configurational potential energy, U, of N particles can be written as

$$U = \sum_{i>j} u(r_{ij}) \tag{27}$$

where r_{ij} ($=|\underset{\sim}{r}_j - \underset{\sim}{r}_i|$) is the distance between the centers of particles i and j. The total force on a particle is obtained as usual from the gradient of the potential:

$$\underset{\sim}{F}_i = -\underset{\sim}{\nabla}_i U = -\sum_{j\neq i} \underset{\sim}{\nabla}_i u(r_{ij}) = \sum_{j\neq i} \underset{\sim}{F}_{ij}$$

3.2 AQUEOUS SYSTEMS

For the aqueous suspensions studied here, only repulsive forces due to the overlap of electrical double layers were considered. The range of the pair interactions is characterized by the familiar Debye screening length κ^{-1},

$$\kappa = e\left(\frac{2cN_A}{\varepsilon kT}\right)^{1/2} \tag{28}$$

where e is the electronic charge (1.602×10^{-19}C), c is the monovalent electrolyte concentration, ε is the electrical permittivity of the aqueous phase (7.08×10^{-10} F/m), and N_A is Avogadro's number.

When the electrolyte concentration and particle diameter are such that $\kappa d<3$, a good approximation for $u(r_{ij})$ is the screened Coulomb (or Yukawa) potential,[22,29,42a]

$$u(r) = \pi\varepsilon(d\psi_o)^2 \{\exp[-\kappa(r-d)]\}/r \tag{29}$$

where ψ_o is the electrical potential at the particle surface.

When $\kappa d>3$ a better approximation to $u(r)$ is given by[22,29]

$$u(r)= \pi\varepsilon d\psi_o^2 \ln\{1+\exp[-\kappa(r-d)]\} \tag{30}$$

under conditions of constant surface potential. This potential was used in simulations of concentrated aqueous dispersions of 1.2 μm diameter spheres at two electrolyte concentrations: 10^{-4} mol/dm^3 and 10^{-6} mol/dm^3. Plots of Eq. (30) for these conditions are shown in Fig. 5.

3.3 NONAQUEOUS SYSTEMS

For the nonaqueous dispersions studied here, the pair potential was taken to be the sum of a repulsive piece arising from steric stabilization and an attractive piece due to van der Waals forces:

$$u(r) = u_S(r) + u_A(r) \tag{31}$$

Steric stabilization arises from the repulsive interaction of polymer layers adsorbed on or bound to particle surfaces. The steeply repulsive potential derived by Ottewill and Walker[34] was used:

$$u_s(r) = \frac{\pi kTC_p^2}{6v_1\rho_p^2}(\psi-\chi)(2R_o + r)(R_o - r)^2 \tag{32}$$

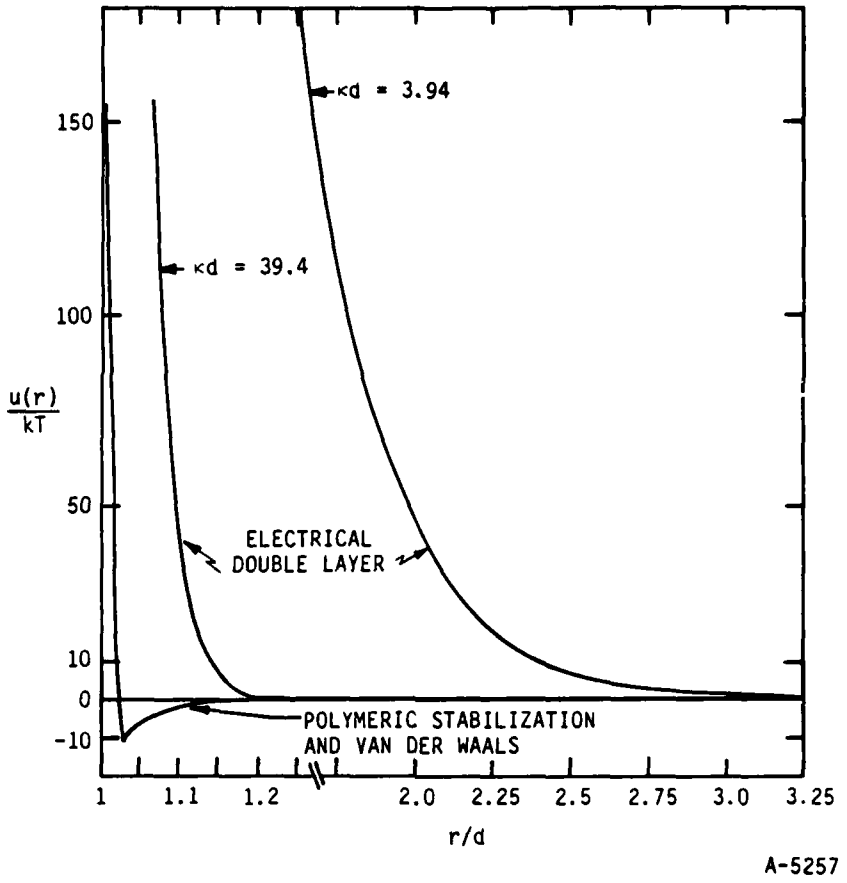

Figure 5. Potentials used for simulating concentrated dispersions.

where

$$R_o = d + 2\delta \quad .$$

The thickness of the adsorbed polymer layer is denoted by δ, and R_o is the distance at which the steric repulsive force is first felt. In the simulation runs, a layer thickness of 0.02 μm was used and a value of 0.013 g/cm^3 was used for C_p, the concentration of polymer segments per unit volume of the adsorbed layer. The remaining parameters were evaluated following Cairns, Van Megan and Ottewill[35] and are appropriate for poly (12-hydroxystearic acid) chains with a dodecane solvent. The density ρ_p of the adsorbed chains is 1.114 g/cm^3, the difference between the entropic (ψ) and enthalpic (χ) interaction parameters is 0.3, and the partial molar volume v_1 of the solvent is 227.3 cm^3/mol.

The attractive potential between two spheres, neglecting retardation effects, was derived by Hamaker:[36]

$$u_A(r) = -\frac{A}{12}\left[\frac{d^2}{r^2 - d^2} + \frac{d^2}{r^2} + 2\ell n\left(\frac{r^2 - d^2}{r^2}\right)\right] \qquad (33)$$

A value of 5.0×10^{-20}J was used for the Hamaker constant, A. A plot of Eq. (31) is shown in Fig. 5.

4. RESULTS AND DISCUSSION

4.1 EQUILIBRIUM SIMULATIONS

Equilibrium simulations of concentrated suspensions of 1.2 μm diameter spheres were performed. Aqueous suspensions at volume fractions of 0.15, 0.25, and 0.35 were studied using the potential given by Eq.(30) with $\psi = 0.06V$ and $c = 10^{-4}$ mol/dm^3. At this electrolyte concentration, the screening length κ^{-1} is about 0.03 μm, and $\kappa d = 39.4$. This results in the relatively short-ranged, repulsive potential shown in Figure 5. A nonaqueous suspension of sterically stabilized 1.2 μm diameter spheres was simulated at a volume fraction of 0.40 using the potential given by Eqs. (31) to (33). This potential has a deep primary minimum (not shown) for $r/d < 1.005$ and a shallow secondary minimum at $r/d = 1.033$ separated by a steeply repulsive wall that prevents irreversible coagulation into the primary minimum. The potential is shown in Fig. 5.

Figures 6 through 9 contain the results for the aqueous suspensions. All calculations were performed using 32 particles and a time step of 2×10^{-4}s. Figure 6 compares the calculated g(r) at $\phi = 0.35$ with the result of Van Megen and Snook.[30] The agreement is very good. Figure 7 shows the progressive change in the equilibrium structure that occurs as the volume fraction decreases. The prominent nearest neighbor peak when $\phi = 0.35$ arises from the strong repulsions that prevent particles from approaching each other too closely. This peak shrinks rapidly as ϕ decreases because the particles have more free volume in which to move. The excluded particle region around $r/d = 1.55$ is evidence that when $\phi = 0.35$ the suspension has a high degree of solid-like order. This feature disappears as ϕ decreases. At $\phi = 0.25$, g(r) is liquid-like, and at $\phi = 0.15$, the suspension structure is beginning to resemble that of a repulsive soft-sphere gas. In Figs. 8 and 9, the m.s.d. and self-diffusion coefficient strongly show the effects of increasing ϕ. Van Megen's and Snook's[30] results in Figs. 8 and 9 also illustrate the influence hydrodynamic interactions have in determining the short time diffusive motion of the particles.

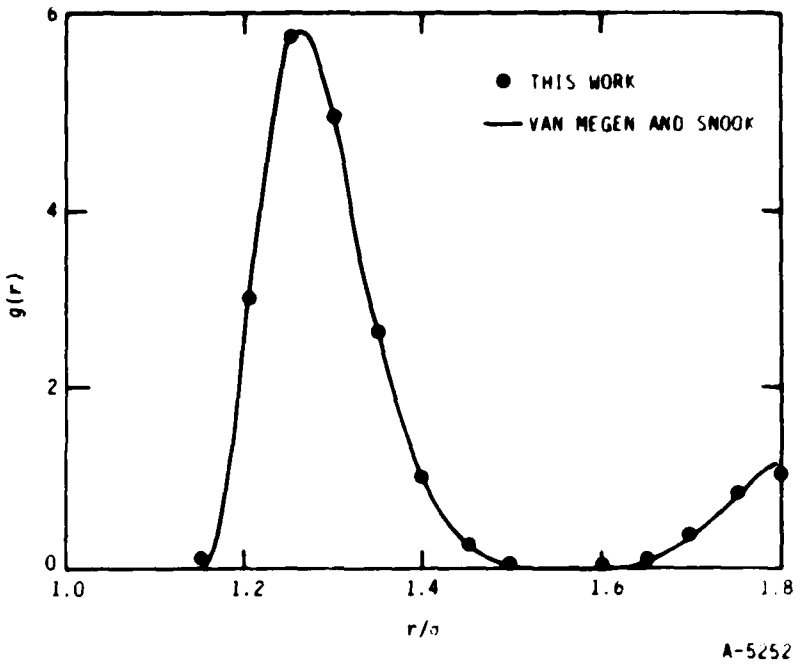

Figure 6. Radial distribution function for dispersion with $\kappa d = 39.4$ at $\phi = 0.35$ (from Ref. 30).

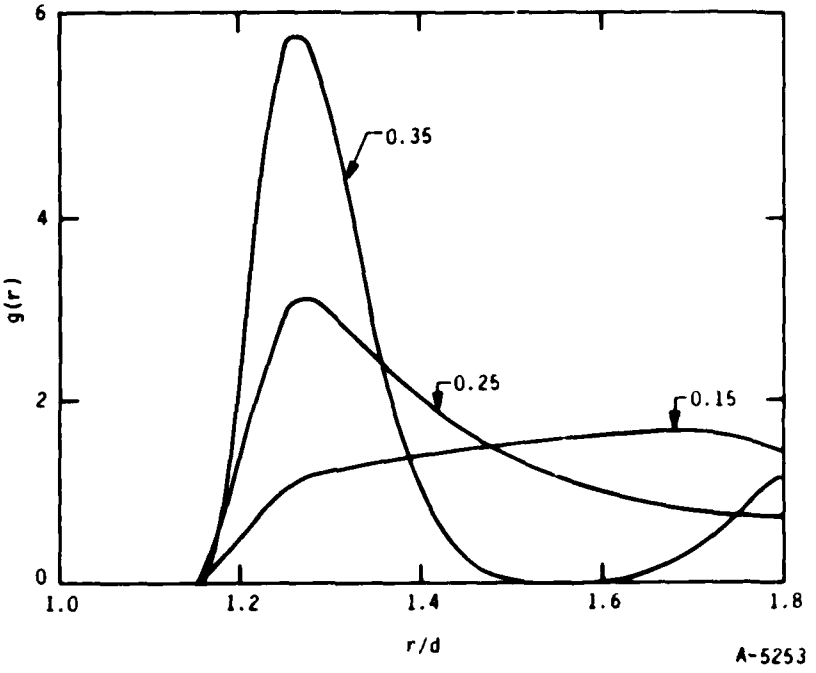

Figure 7. Radial distribution functions for dispersions with $\kappa d = 39.4$ at $\phi = 0.15$, 0.25, and 0.35.

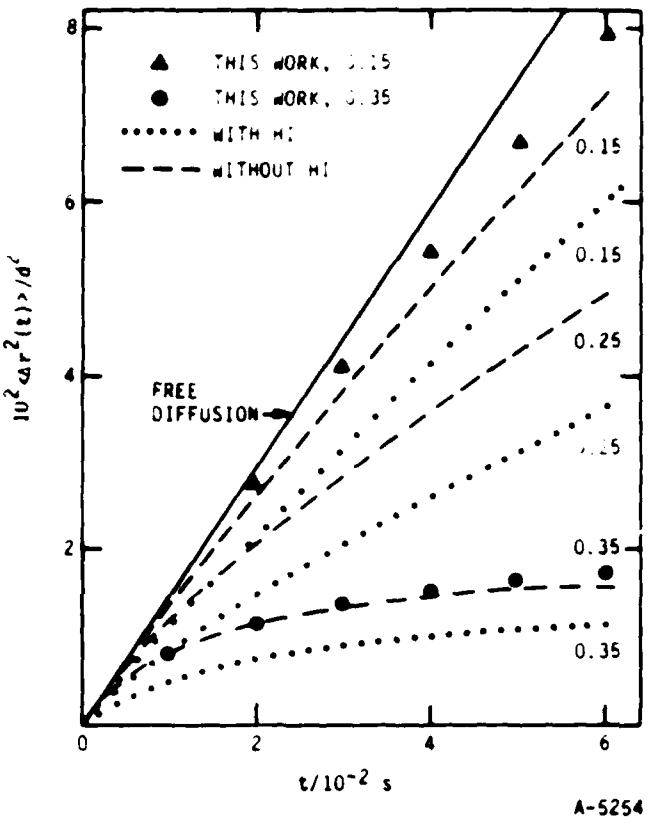

Figure 8. Plot of the mean square displacement against time for dispersion with n = 0.1 mol m^{-3}, Van Megen's and Snooks' results with hydrodynamic interactions (•••) and those neglecting hydrodynamic interactions (---). The values alongside the curves denote the volume fraction. (After Ref. 30.)

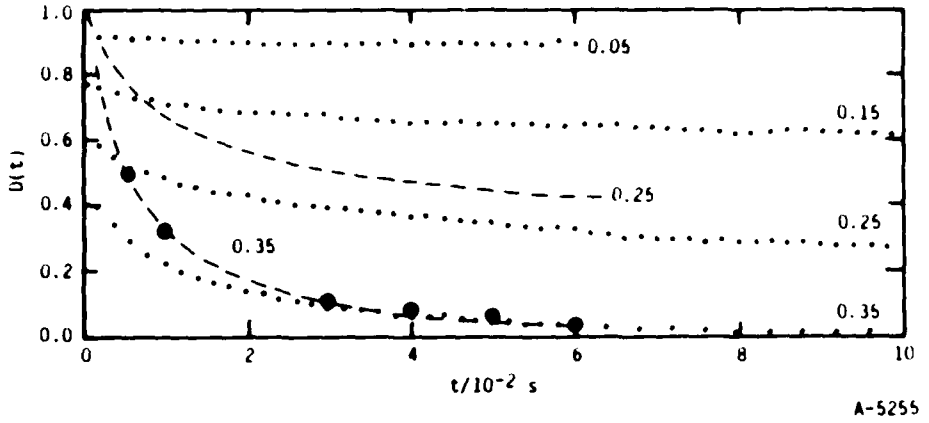

Figure 9. Plot of the time-dependent self-diffusion constant (Eq. (23)), expressed in units of D_o, against time. Other details as for Figure 8 (after Ref. 30).

The simulation of the nonaqueous suspension was done using 108 particles and, due to the hardness of the repulsive potential, a time step of 5×10^{-6}s. In Fig. 10, g(r) for the nonaqueous suspension at $\phi = 0.4$ is shown. The most significant feature is the very strong nearest neighbor peak. This peak is considerably sharper than those found for the aqueous suspensions. This is due to the hardness and shorter range of the nonaqueous repulsive potential in combination with the secondary attractive well. The peak thus represents weakly flocculated particles with separations narrowly distributed about the secondary minimum. Each particle has, on average, six very near neighbors with r/d lying between 1.03 and 1.06. The self-diffusion coefficient for this system has a very rapid decay (not shown), dropping to 47 percent of D_o after only 10^{-4}s and to 12 percent of D_o after 10^{-3}s. The asymptotic value of about 0.09 D_o is reached after 3×10^{-3}s. This decay is much faster than that seen in Fig. 9 for the aqueous suspensions and is probably a consequence of caging due to the weak flocculation or perhaps to the slower collective motion of weakly bound groups of particles.

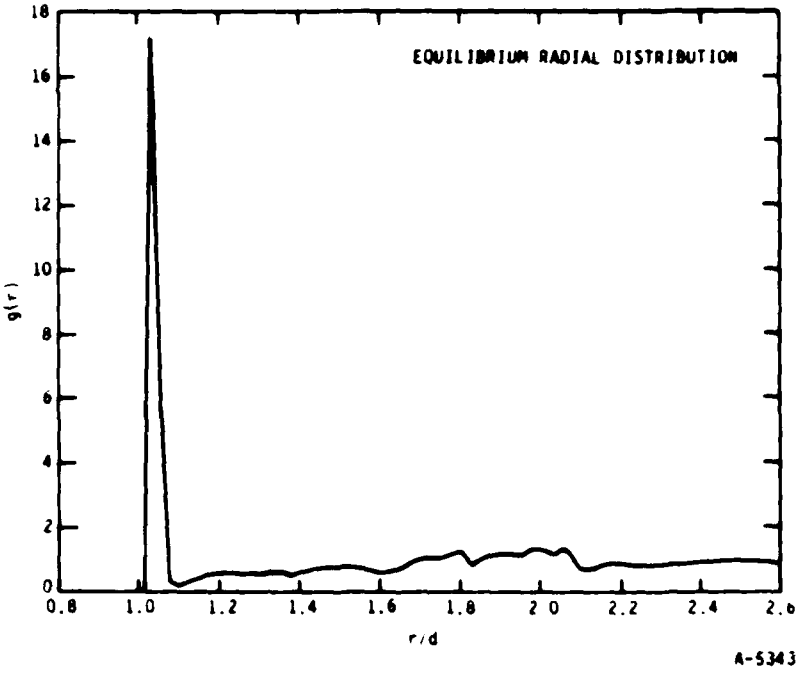

Figure 10. Equilibrium radial distribution function for nonaqueous dispersion with $\phi = 0.4$

4.2 NONEQUILIBRIUM SIMULATIONS

Simulations were performed with 108 particles for volume fractions of 0.2 or 0.4, except for one run with $\phi = 0.35$, at various shear rates ranging from 5 to 200s^{-1}. The particle diameter was always 1.2 μm. Three different potentials were used in order to assess the effect of interparticle forces on shear thinning. Two of these were also used for the equilibrium simulations just described. The third potential is given by Eq. (30) with $\psi = 0.06V$ and with $c = 10^{-6}$ mol/dm^3. At this electrolyte concentration the Debye screening length is increased by a factor of ten over the value used for the equilibrium simulations. With this increase, κd now equals 3.94, and the range of the repulsive, electrostatic stabilization potential is substantially extended. This is apparent in Fig. 5, where all three potentials are plotted.

Generally, the first five to ten thousand time steps of a run were used to bring the system to steady state. The run would then be continued for another twenty to thirty thousand time steps, during which g(r), the average of the particle stress tensor (Eq. (26)) and its square were computed. The computations were performed on PSI's in-house DEC MicroVax II computer system. In order to reduce the computational time needed for these preliminary studies, random numbers with a uniform, rather than Gaussian, distribution were generated over the interval (-1/2, +1/2). A test run showed this to have only a small effect on the calculated results. For 108 particles, 1700 time steps could be performed per CPU hour. A typical 20,000 step run would then require about 12 hrs of computer time. For the nonaqueous systems, the same time step (5×10^{-6}s) used in the equilibrium simulations proved satisfactory. A time step of 2×10^{-5}s was used for simulating the aqueous suspensions. This is one-tenth of the value used for the equilibrium simulations. The smaller time step was needed to avoid artificially bringing pairs of particles into highly repulsive configurations that would result in unphysically large displacements on the subsequent time step. This can occur because with the relatively soft repulsive potentials used for the aqueous systems studied here, the effect of shear is to drive some of the particles closer together where they experience stronger repulsions than at equilibrium.

This can be seen in Fig. 11 where the equilibrium g(r) and the angular-averaged nonequilibrium g(r) are plotted for an aqueous suspension with $\phi = 0.35$ and $\kappa d = 39.4$. Besides driving particles closer together, shear reduces the number of particles in the nearest neighbor shell, spreading them over a wider range of pair separations. This is evident from the appearance of particles in the range $1.45 < r/d < 1.65$ where they were strongly excluded at equilibrium. Thus the average particle distribution is more uniform than at equilibrium, although it should be noted that in a sheared suspension g(r) is strongly angular dependent and not spherically symmetric as at equilibrium.

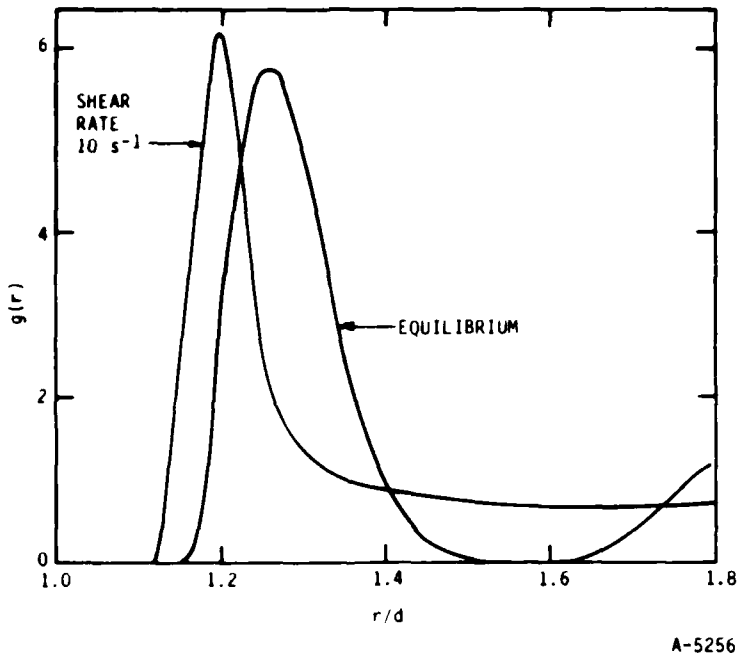

Figure 11. Radial distribution functions for dispersion with $\kappa = 39.4$ at $\phi = 0.35$, at equilibrium and at a shear rate of $10s^{-1}$.

The behavior of the sheared nonaqueous suspensions is somewhat different. Figures 12 through 14 show the angular-averaged nonequilibrium g(r) for $\phi = 0.4$ at three different shear rates: 20, 100, and $200s^{-1}$. The very hard repulsive part of the potential for these systems prevents any significant decrease in the minimum pair separation at the shear rates studied. The high steric barrier also makes it virtually impossible for shear-induced coagulation

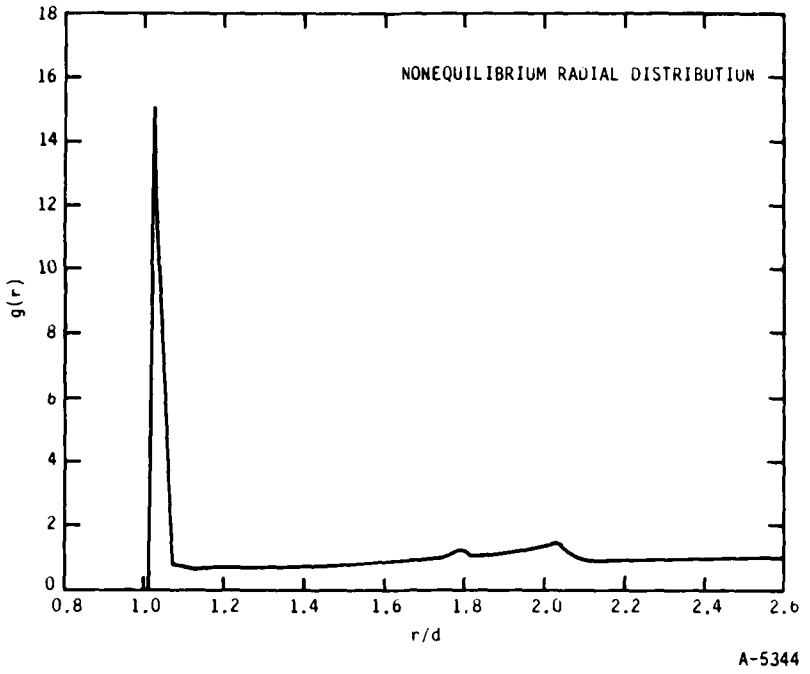

Figure 12. Nonequilibrium radial distribution function for nonaqueous dispersion with ϕ = 0.4 and shear rate of $20s^{-1}$.

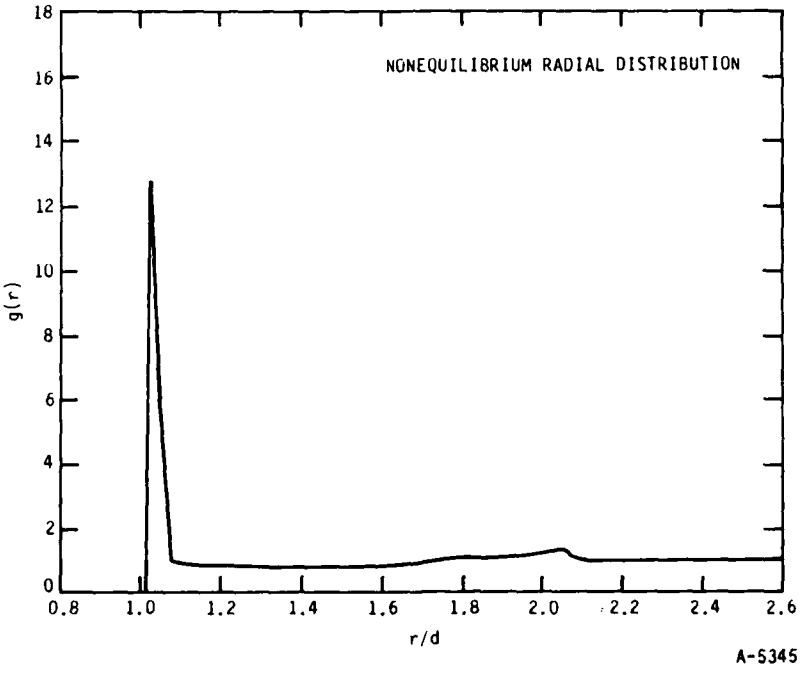

Figure 13. Nonequilibrium radial distribution function for nonaqueous dispersion with ϕ = 0.4 and shear rate of $100s^{-1}$.

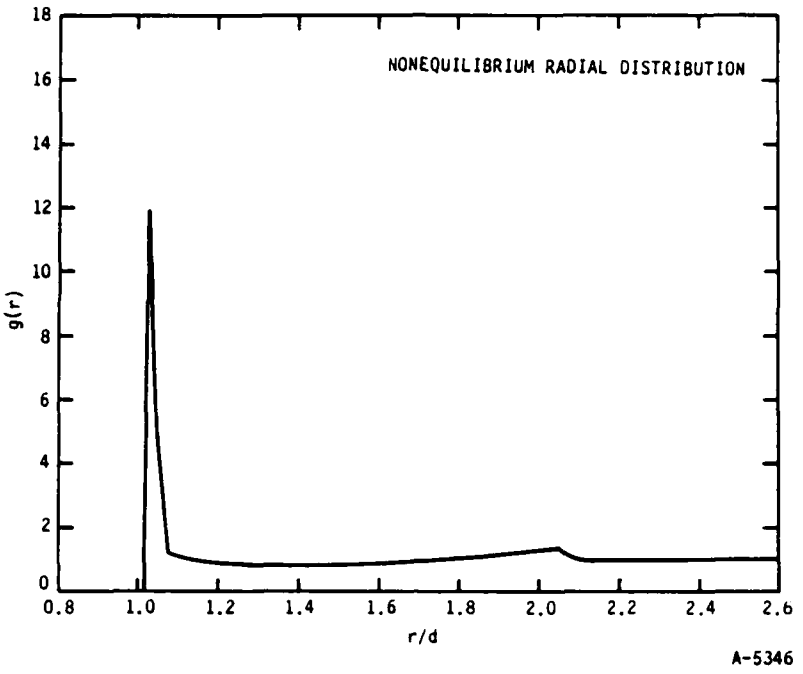

Figure 14. Nonequilibrium radial distribution function for nonaqueous dispersion with $\phi = 0.4$ and shear rate of $200s^{-1}$.

to occur at these shear rates. Thus the only significant effect of shear observed here is to reduce substantially the number of nearest neighbors around any particle. This is demonstrated by the marked reduction in height of the major peak as the shear rate increases. Compared to the equilibrium g(r) in Fig. 10, the sheared particle distribution is more uniform at larger r as well. Minor structural features in the equilibrium curve are steadily reduced with increasing shear rate.

Figures 15 through 22 illustrate the calculated volume fraction and shear rate dependence of the relative viscosity of the various suspensions. Some comparisons with experimental data are also given. The relative viscosity η_r of the suspension is defined as the ratio of the measured or calculated suspension viscosity to the viscosity of the pure suspending fluid,

$$\eta_r = \eta/\eta_o \quad . \tag{34}$$

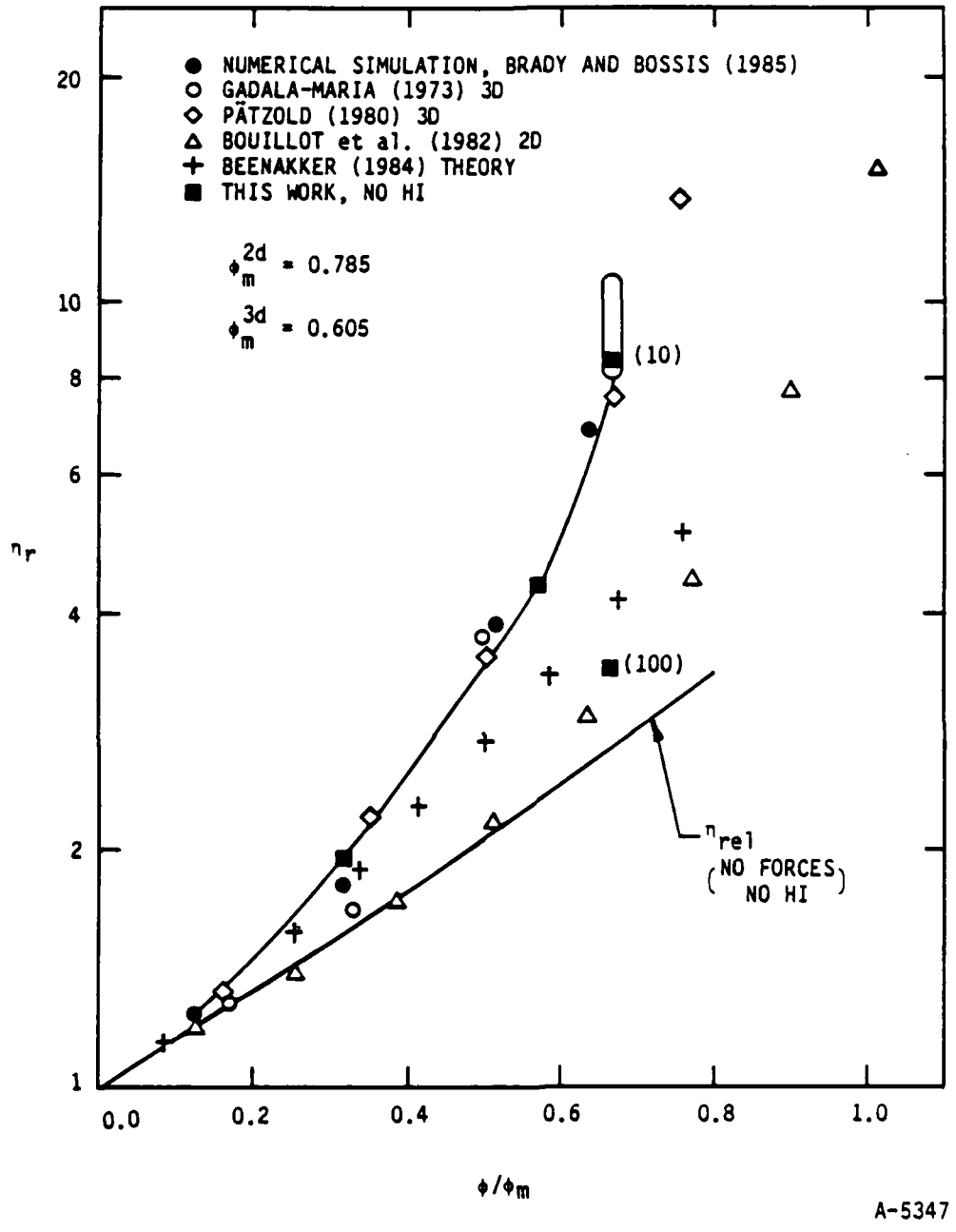

Figure 15. Volume fraction dependence of relative viscosity for hard sphere suspensions (from Ref. 8)

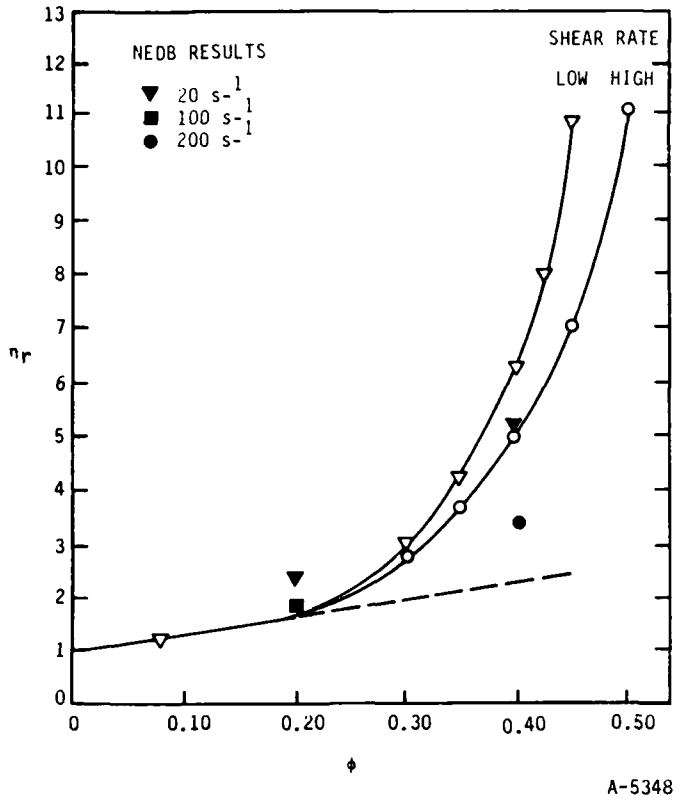

Figure 16. The non-Newtonian behavior of nonaqueous latices at high volume fractions. Open symbols: data from Ref. 37. Solid symbols: NEBD results for nonaqueous dispersion.

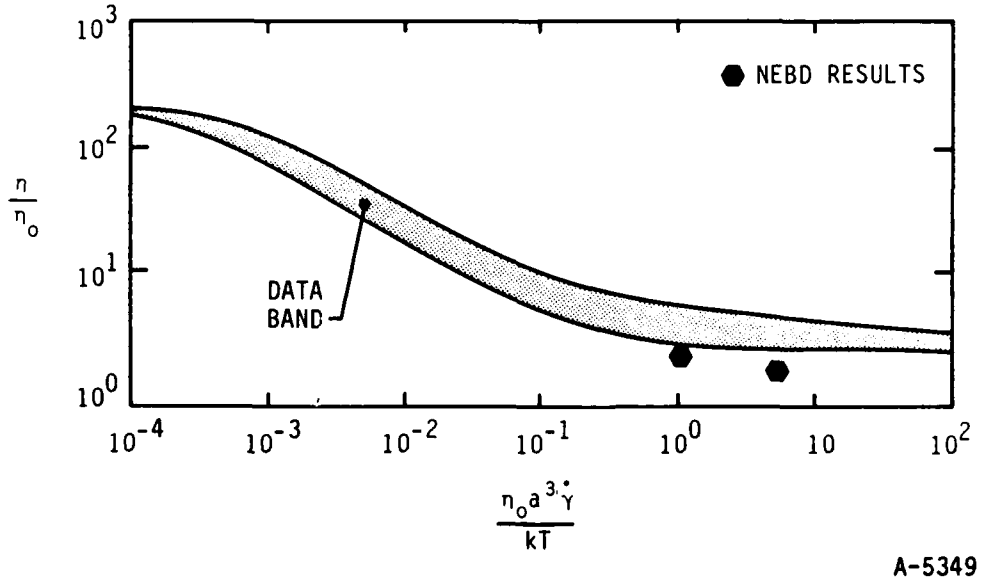

Figure 17. Relative viscosity versus Peclet number for sterically stabilized monodisperse polyvinyl chloride spheres in several solvents at $\phi = 0.20$ (Ref. 38).

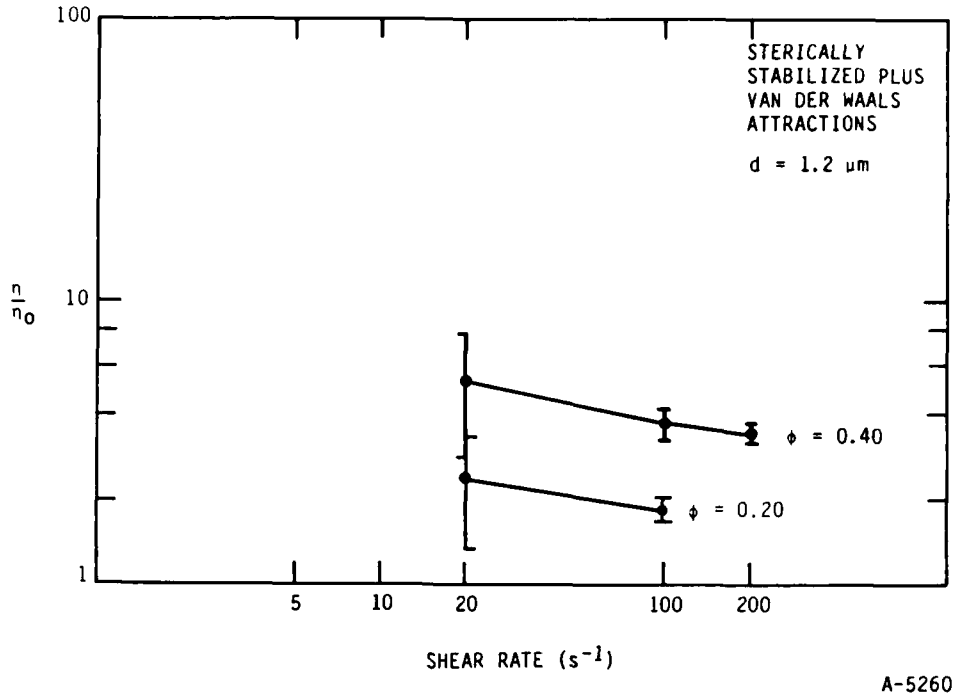

Figure 18. NEBD results for shear rate dependence of viscosity of concentrated dispersions.

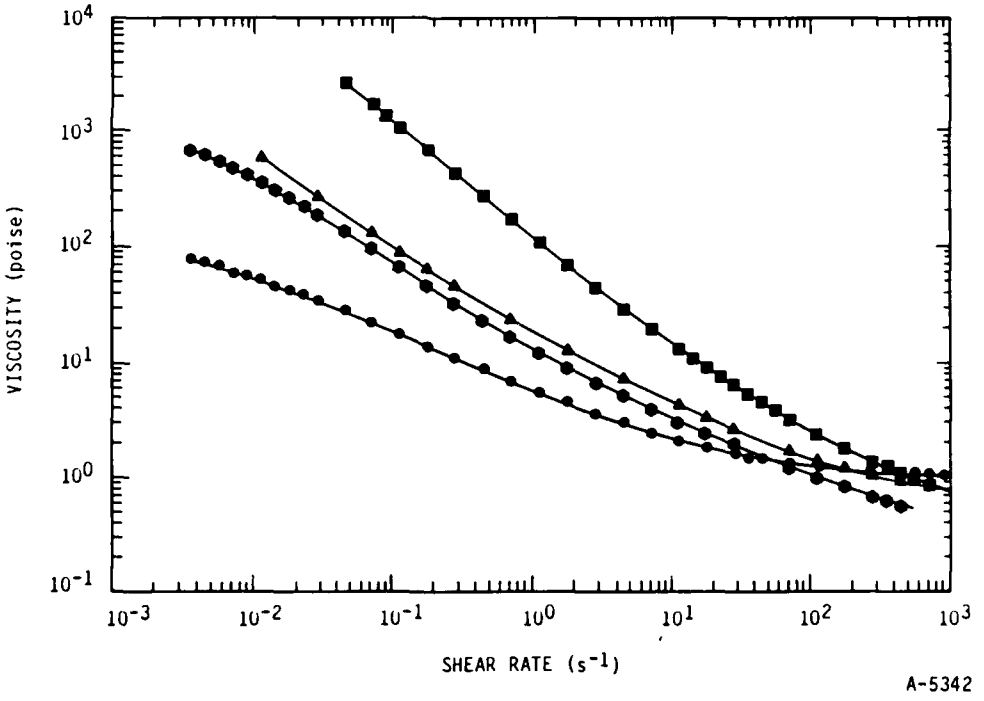

Figure 19. Apparent viscosities of several carbon/hydrocarbon slurry fuel samples (from Ref. 39).

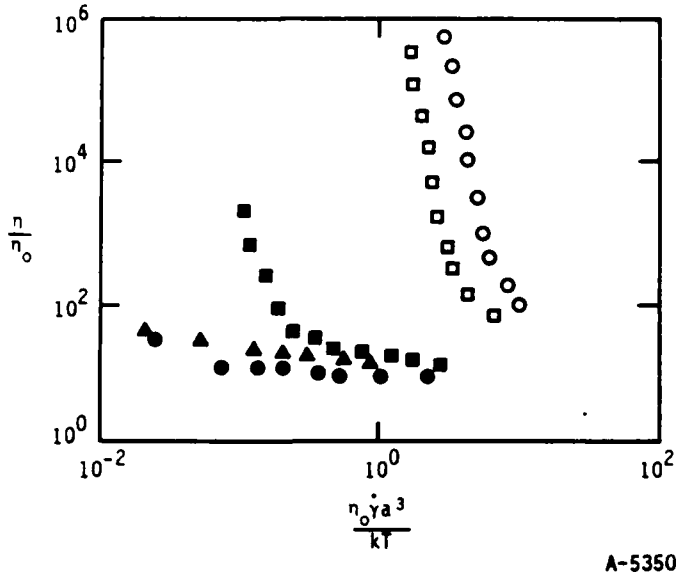

Figure 20. Effect of added electrolyte on the relative viscosity of polystyrene latex suspension with a = 0.11 μm at ϕ = 0.40 (Ref. 40): o deionized; □ 1.876 x 10^{-4}M HCl; ■ 1.876 x 10^{-3}M HCl; ▲ 1.876 10^{-2}M HCl; ● 9.378 x 10^{-2}M HCl. (From Ref. 2).

Figure 15 is adapted from the paper of Brady and Bossis.[8] It shows the volume fraction dependence of η_r for several experimental systems, theoretical results of Beenakker,[41] and their Stokesian dynamics (SD) simulations. Our low shear ($10s^{-1}$) results for aqueous suspensions with κd = 39.4 at ϕ = 0.2, 0.35, and 0.4 have been added to the figure. A higher shear rate ($100s^{-1}$) value for ϕ = 0.4 is also included. The figure was originally intended to compare values for hard sphere suspensions, thus our values are not strictly comparable with the others. However, they do demonstrate that NEBD simulations of moderately repulsive spheres do produce a dependence on ϕ that corresponds well with observed behavior on related systems. Our higher shear rate value for ϕ = 0.4 shows a considerable shear thinning effect; more discussion of this point will follow shortly. The lower line added to the figure represents the relative viscosity due only to the solvent and independent particle hydrodynamic contributions. It neglects interparticle forces and hydrodynamic interactions. It is clear that interparticle forces contribute to our NEBD results to about the same degree that hydrodynamic interactions contribute to the force-free SD results of Brady and Bossis.[8] Brady and Bossis[8] also simulated a system with a much shorter-ranged, more highly repulsive potential

than used in any of the present aqueous simulations. This system showed a very weak shear-thinning effect, and exhibited a slight shear thickening at much higher shear rates due to hydrodynamic interactions.

Figure 16 presents the volume fraction dependence of η_r for nonaqueous latices in the high and low shear rate limit.[37] Also shown are our NEBD results for $\phi = 0.2$ and 0.4 at shear rates of 20 and $200s^{-1}$. The discrepancy at $\phi = 0.4$ is almost entirely due to the lack of hydrodynamic interactions between particles in the simulations, but the shear thinning effect, due to interparticle forces, is reproduced reasonably well. Hydrodynamic interactions are relatively unimportant for the more dilute dispersion, which also shows very little shear thinning at these shear rates. Figure 17 is a compendium of data[38] on nonaqueous dispersions at $\phi = 0.2$ taken from a review by Russel.[2] When plotted against a dimensionless shear rate, the Péclet number $n_o a^3 \dot{\gamma}/kT$, the relative viscosity data for different particle sizes lie on a single curve. Shear thinning is evident at very low dimensionless shear rates. This apparent conflict with the experimental results shown in Fig. 16 may be due to some relatively weak, long ranged interaction or structure formation that is important only at very low shear rates. The available NEBD results plotted in Fig. 17 are in reasonable agreement with the data, but it was not possible to explore the shear thinning region. Meaningful results could not be obtained at lower shear rates due to large statistical fluctuations for the 108 particle system studied. Even for the two points shown, the standard deviation for the average particle stress contribution to η_r was comparable to the average value.

Figure 18 shows the shear rate dependence of the two nonaqueous dispersions calculated from the NEBD simulations. The error bars indicate the calculated standard deviations. It is gratifying that the NEBD simulations of the model nonaqueous system correspond well with data for real systems. It is also worth noting how much lower the viscosity of well-stabilized dispersions is compared to that of carbon/hydrocarbon fuel slurries, such as reported by Lin and Brodkey.[38] An example of their results is shown in Fig. 19. These systems apparently have either a long-range network structure or a strong

shorter-ranged structure that leads to very high viscosities at low shear rates, to pronounced shear thinning behavior, and to high relative viscosities (≈100) even at shear rates greater than $100s^{-1}$. It seems reasonable to infer that improved polymeric stabilization techniques could greatly reduce the viscosities of these fuel slurries.

Although it was not possible to simulate either long or short range structural effects in nonaqueous suspensions during the Phase I program, a crude analog for this, termed the secondary electroviscous effect, was simulated in the aqueous system studies. This effect refers to the increase in viscosity of aqueous dispersions that occurs when the electrolyte concentration is progressively reduced. The phenomenon is illustrated with experimental results[40] in Fig. 20. At fixed particle volume fraction, the increasing Debye screening length results in much longer ranged forces, and the system becomes much more strongly interacting. Although this is clearly not the same type of strong interaction or long range structural effect assumed to be acting in the highly viscous nonaqueous slurry, it is nevertheless a valuable confirmation of the applicability of the NEBD method to a strongly interacting system with long ranged forces.

The results of the calculations are shown in Fig. 21. Aqueous dispersions with $\phi = 0.2$ and $\kappa d = 39.4$ and 3.94 were simulated. The change in κ is due to a hundred-fold reduction in the salt concentration. The minimal shear thinning exhibited by the system with the much shorter ranged potential contrasts sharply with the behavior of the dispersion with long ranged forces. The shear rate dependence of η_r for this latter system is so strong that below shear rates of $10s^{-1}$, its viscosity exceeds that of a suspension at twice the volume fraction ($\phi = 0.4$) with the shorter ranged repulsive forces ($\kappa d = 39.4$). These latter results are plotted in Fig. 22. This system exhibits noticeable shear thinning at $\phi = 0.4$, compared to the minimal effect observed at $\phi = 0.2$, and the effect here is due to crowding particles more closely together. Reducing the interparticle spacing at fixed range of potential is roughly equivalent to increasing the range of the potential at fixed volume fraction. Both changes result in a more strongly interacting system, and that gives rise to an increase in the viscosity.

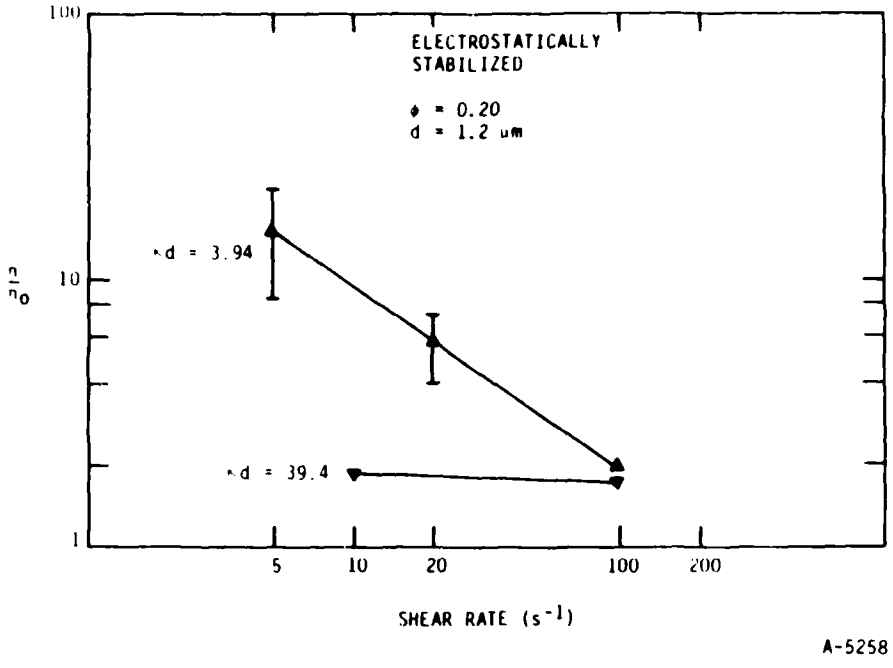

Figure 21. NEBD results for shear rate dependence of viscosity of concentrated dispersions.

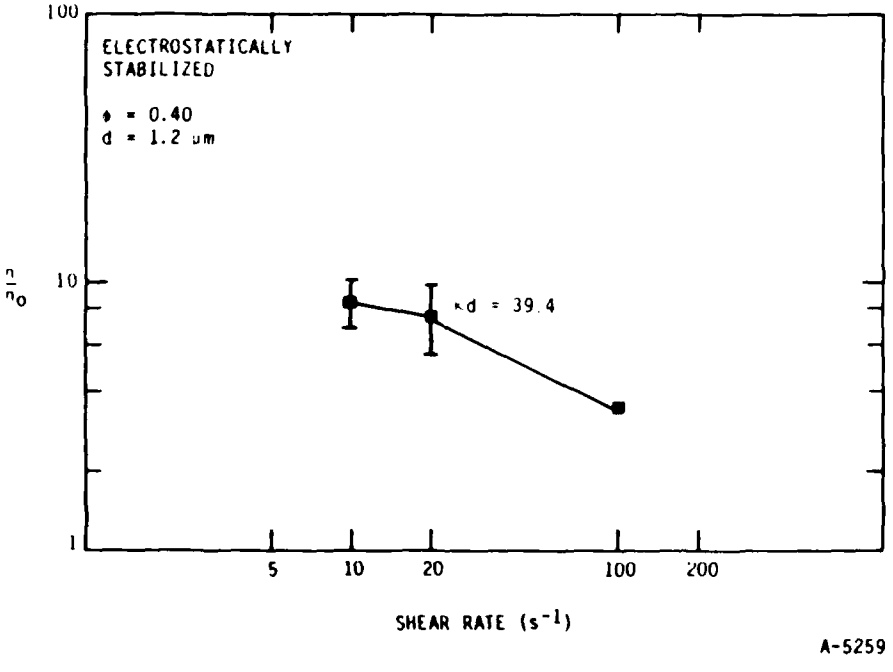

Figure 22. NEBD results for shear rate dependence of viscosity of concentrated dispersions.

Based on the small number of cases studied, the following tentative conclusions may be offered regarding the effect of interparticle forces on shear thinning. With increasing shear, the average number of near neighbors to any particle decreases and the average number of particles with larger separations grows. Both trends result in a decreased contribution to the average particle stress term and, thus, to a lower viscosity. Dispersions with harder, short ranged forces (even with long ranged, but weak attractions) show less shear thinning than ones with longer ranged strong interactions simply because the former systems have less "viscosity" to lose at any volume fraction. The system whose dominant interactions are short ranged generates significant contributions to the average particle stress only from very close pairs. In the system with a longer ranged strong interaction, the stress receives contributions from a broader range of particle separations and, consequently, is larger. At sufficiently high shear rates, the particle distribution is so spread out that the force contribution to the stress is dominated by convection. A complete discussion of shear thinning would include the effects of hydrodyamic interactions,[7,8] which become more important at higher shear rates.[44] Since these were not included in the Phase I feasibility study, no speculation will be offered regarding them.

4.3 CLASSICAL STABILITY ESTIMATES

Classical colloid stability estimates are based on the application of Fuchs' well known theory[45] for the rate of diffusion of particles over a potential barrier. The ratio of the rates without and with the barrier is termed the stability ratio, W. This is defined as

$$W = d \int_{d}^{\infty} \exp\left(\frac{u(r)}{kT}\right)/r^2 dr \qquad (35)$$

The nonaqueous system is of primary interest here, and the appropriate potential is given by Eqs. (31) through (33). For parameter values of interest, this potential is very sharply peaked at a value of r, say r_m, that is just slightly greater than d. Because of this, the exponential function in

Eq. (35) acts like a delta function, and a quadratic expansion of u(r) is sufficient to accurately approximate the integral via a Gaussian quadrature. The result is

$$W = \exp(u_m/kT)/(d\sqrt{(v''_m/2\pi kT)}) \tag{36}$$

where $u_m = u(r_m)$ and

$$v''_m = -(d^2u/dr^2)\,|\,r = r_m$$

Consider how stability is affected by the strength of the repulsive and attractive parts of the potential. For this exercise, the adsorbed polymer concentration C_p will be used as the key parameter controlling the strength of the repulsive steric potential. The Hamaker constant A (Eq. (33)) is the natural choice for the attractive potential. This quantity depends on the nature of two interacting particles as well as on the intervening fluid medium, and is not a free parameter. Tabor[46] indicates that metallic particles may have A values 5 to 10 times larger than those found for dielectric materials, so variations in A may be regarded as corresponding to changes in the material composition of the dispersed particles.

Smoluchowski's theory of rapid coagulation may be used to estimate the coagulation time t_c,

$$t_c = 3n_o/(4kT\rho)$$

With the value $\rho = 10^{12}/cm^3$ for 1 μm diameter particles at a volume fraction of 0.4, the coagulation time is of the order of 0.2s. This coagulation time must be increased by about a factor of 10^8 if stability for a year (3×10^7s) is desired. Consequently, when W exceeds 10^8, reasonable stability is insured; for W smaller than 10^8, coagulation proceeds at a faster rate. Because ρ varies as d^{-3} at fixed ϕ, smaller particles require larger values of W to insure comparable periods of stability. It is well known that suspensions of small particles are generally more difficult to stabilize than those of larger particles.[22]

Values of the stability ratio are shown in Table 1 for different combinations of C_p and A. Not surprisingly, the results show that decreases in C_p or increases in A result in decreased colloidal stability. Less adsorbed polymer means a less effective steric barrier. An increased attractive potential also reduces the repulsive barrier height. In a given system, A will be fixed, and stability can be enhanced by increasing the amount of polymer adsorbed. It should be noted that A depends, in principle, on the amount of adsorbed polymer, but this effect should be negligible for particle sizes of interest due to the relatively small amounts of polymer involved.

TABLE 1. Stability Ratio W, Potential Height u_m, and curvature v_m'' at r_m for Different Concentrations of Adsorbed Polymer and Hamaker Constants.

C_p (10^{-2} g/cm^3)	A (10^{-20} J)	u_m/kT	$a^2 v_m''/2kT$	W	Stable/ Unstable
1.3	5.0	154.2	3.38×10^6	9.0×10^{63}	S*
1.0	5.0	61.3	1.39×10^6	6.4×10^{23}	S
0.95	5.0	49.4	1.38×10^6	4.3×10^{18}	S
0.90	5.0	38.5	1.14×10^6	8.7×10^{13}	S
0.85	5.0	28.6	0.83×10^6	5.1×10^9	S
0.80	5.0	19.8	0.71×10^6	8.0×10^5	U
0.75	5.0	11.9	0.61×10^6	3.3×10^2	U
0.75	1.0	64.5	1.71×10^6	1.4×10^{25}	S
0.65	1.0	43.1	0.90×10^6	3.2×10^{14}	S
0.55	1.0	25.8	0.53×10^6	4.0×10^8	S
0.45	1.0	12.6	0.33×10^6	8.9×10^2	U
0.40	1.0	7.5	0.20×10^6	7.0	U
0.40	0.5	14.2	0.34×10^6	4.3×10^3	U
0.50	0.5	27.4	0.61×10^6	1.9×10^9	S
0.55	0.5	35.6	0.86×10^6	5.5×10^{12}	S

*System used for computer simulations.

5. SUMMARY AND CONCLUSIONS

A number of equilibrium and nonequilibrium Brownian dynamics (NEBD) simulations of concentrated colloidal suspensions have been performed. Both aqueous and nonaqueous suspensions have been studied. Stability estimates for sterically stabilized nonaqueous suspensions have been made. These results can be understood in terms of the changes occurring in the repulsive steric potential and attractive van der Waals potential as the adsorbed polymer concentration and Hamaker constant are changed. Quantitative evidence for the disturbance of the equilibrium structure of the dispersions by shearing has been obtained. Shear viscosities of suspensions have been calculated as a function of shear rate and particle volume fraction. With allowance for the neglect of hydrodynamic interactions, good agreement was obtained with experimental viscosities for comparable systems. The simulation results are sensitive to the type, strength and range of the potential interactions used to describe the dispersion. The overall conclusion of this Phase I study is that the NEBD technique is capable of describing the essential features of sheared suspension behavior. These Phase I results establish the feasibility and desirability of using NEBD simulation methods as a predictive engineering tool for the design of slurries.

6. REFERENCES

1. Jeffrey, D.J. and Acrivos, A., AIChE Journal 22, 417 (1976).

2. Russel, W.B., in Theory of Dispersed Multiphase Flow (Academic, London 1983), p. 1.

3. Goodwin, J.W., in Colloid Science, Volume 2 (Specialist Periodical Reports) ed. D.H. Everett (The Chemical Society, London, 1975), p246.

4. Goodwin, J.W., in Colloidal Dispersions, ed. J.W. Goodwin (Royal Society of Chemistry, London 1982), p. 165.

5. Hirtzel, C.S. and Rajagopalan, R., Colloidal Phenomena (Noyes, Park Ridge, New Jersey) 1985).

6. Ansel, G.C., Dickinson, E., and Ludvigsen, M., J. Chem. Soc., Faraday Trans. 2, 81, 1269 (1985).

7. Bossis, G. and Brady, J.F., J. Chem. Phys. 80, 5141 (1984).

8. Brady, J. and Bossis, G., J. Fluid Mech., 155, 105 (1985).

9. Hoover, W.G., Ann. Rev. Phys. Chem. 34, 103 (1983).

10. Evans, D.J., Molec. Phys. 42, 1355 (1981); 37, 1745 (1979).

11. Evans, D.J. and Morriss, G.P., Comput. Phys. Repts. 1, 299 (1984).

12. Heyes, D.M., Montrose, C.J., and Litovitz, T.A., J. Chem. Soc. Faraday Trans. 2, 79, 611 (1983).

13. Hoover, W.G., Molecular Dynamics, Lecture Notes in Physics 258 (Springer-Verlag, Berlin, 1986).

14. Ermak, D.L., J. Chem. Phys. 62, 4189, 4197 (1975).

15. Doll, J.D. and Dion, D.R., Chem. Phys. Lett. 37, 386 (1976).

16. Turq, P., Lantelme, F., and Friedman, H.L., J. Chem. Phys. 66, 3039 (1977).

17. Ermak, D.L. and McCammon, J.A., J. Chem. Phys. 69, 1352 (1978).

18. Fixman, M., J. Chem. Phys. 69, 1527, 1538 (1978); Macromolecules 14, 1710 (1981).

19. Israelachvili, J.N., Adv. Coll. Interface Sci. 16, 31 (1982).

20. Ninham, B.W., Adv. Coll. Interface Sci. 16, 3 (1982).

21. Napper, D.H., Colloidal Dispersions, ed. J.W. Goodwin (Royal Society of Chemistry, London, 1982), p. 99.

22. Verwey, E.J.W. and Overbeek, J. Th. G., The Theory of the Stability of Lyophobic Colloids (Elsevier, Amsterdam, 1948).

23. Sonntag, H. and Strenge, K., Coagulation and Stability of Disperse Systems (Israel Program for Scientific Translations, Hlasted Press, New York, 1972).

24. Gregory, J., J. Coll. Interface, Sci. 83, 138 (1981).

25. Wilemski, G., J. Coll. Interface, Sci. 88, 111 (1982).

26. Wilemski, G., J. Stat. Phys. 14, 153 (1976).

27. Fincham, D., Comput. Phys. Commun. 21, 247 (1980).

28. Lees, A. and Edwards, S., J. Phys. C 5, 1921 (1972).

29. Van Megen, W. and Snook, I., Faraday Discuss. Chem. Soc. 76, 151 (1983).

30. Van Megen, W. and Snook, I., J. Chem. Soc., Faraday Trans. 2, 80, 383 (1984).

31. Cook, R., Private communication (1986).

32. Ball, R.C. and Richmond, P., Phys. Chem. Liq. 9, 99 (1980).

33. Batchelor, G.K., J. Fluid Mech. 83, 97 (1977).

34. Ottewill, R.H. and Walker, T., Kolloid Z.Z. Polym. 227, 108 (1968).

35. Cairns, R.J.R., Van Megan, W., and Ottewill, R.H., J. Colloid Interface Sci. 79, 511 (1981).

36. Hamaker, H.C. Physica 4, 1058 (1937).

37. Papier, Y.S. and Krieger, I.M., J. Colloid Interface Sci. 34, 126 (1970).

38. Willey, S.J. and Macosko, C.W., J. Rheol. 22, 525 (1978).

39. Lin, S.-F. and Brodkey, R.S., J. Rheol. 29, 147 (1985).

40. Krieger, I.M. and Equiluz, M., Trans. Soc. Rheol. 20, 29 (1976).

41. Beenakker, C.W.J., Physica A 128, 44 (1984).

42. (a) Gaylor, K.J., Snook, I.K., Van Megen W.J., and Watts, R.O., Chem. Phys. 43, 233 (1979); (b) J.C.S. Faraday II 76, 1067 (1980); (c) J. Phys. A 13, 2513 (1980).

43. Snook, I.K., Van Megen, W., Gaylor, K.J., and Watts, R.O., Adv. Coll. Interface Sci. 17, 33 (1982).

44. De Kruif, C.G., Van Iersel, Vrij, A., and Russel, W.B., J. Chem. Phys. 83, 4717 (1985).

45. Fuchs, N.A., Z. Phys. Chem. A171, 199 (1934).

46. Tabor, D., in Colloidal Dispersions, ed. J.W. Goodwin (Royal Society of Chemistry, London 1982), p. 23.

APPENDIX A

EQUILIBRIUM SIMULATIONS OF DILUTE DISPERSIONS

Gaylor, Snook, Van Megen and Watts[29,30,42,43] have published the results of a number of equilibrium Brownian dynamics simulations of colloidal suspensions. In order to verify the satisfactory operation of the present equilibrium code, several simulations were performed for conditions reported in the literature. The potentials used are shown in Figure A-1. Comparisons were made for the radial distribution function, mean square displacement and self-diffusion coefficient. Dilute, but strongly interacting, suspensions were studied. Hydrodynamic interactions were neglected. This is justifiable for the dilute systems.

Comparisons of the present computations for dilute suspensions with those of Gaylor et al.[42a,43] and Van Megen and Snook[29] are shown in Figs. A-2 through A-6. Generally the calculations were done using 32 particles; however those at $\phi = 9.9 \times 10^{-4}$ (Figs. A-5 and A-11) required 256 particles. In general the comparisons are quite favorable. The results of Gaylor et al.[42a] in Fig. A-2 show how changing the ionic strength of the electrolyte affects the structure of the suspension. At the highest concentration, the repulsive potential is relatively short-ranged compared to the average interparticle spacing, and g(r) is characteristic of a very dilute gas with a soft, purely repulsive potential. As the electrolyte concentration decreases, the range of the potential increases. Because the particle volume fraction is constant, the suspension behaves as though it were becoming denser, and g(r) develops its characteristic nearest-neighbor peak due to the excluded volume around each particle. In other words, particles are being pushed away from each other as the repulsive force between them increases. The effect of volume fraction on the time dependence of the m.s.d. and the self-diffusion coefficient as calculated by Gaylor et al. is shown in Figs. 8 and 9. As expected, motion slows with increasing ϕ. These two figures show clearly how the average motion differs at short and long times. Because the average force on a particle is zero, short time motion will be force-free diffusion as described by Eq. (19) with a self-diffusion coefficient equal to D_i. Over long times,

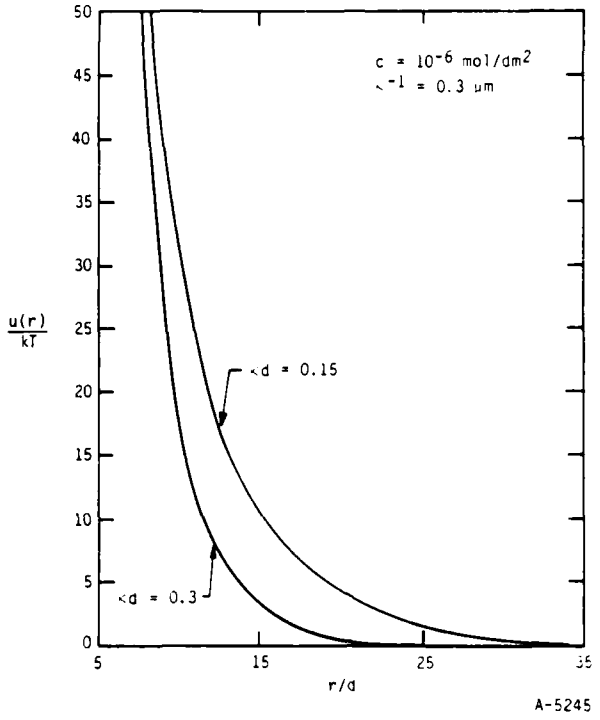

Figure A-1. Repulsive potentials used for simulations of dilute dispersions. Potentials are based on Eq. (29) and are due to electrical double layer interactions in an electrolyte with a concentration of 10^{-6} mol/dm^3. Surface potential ψ_o is 0.22V when d = 0.046 μm and 0.23V when d = 0.09 μm.

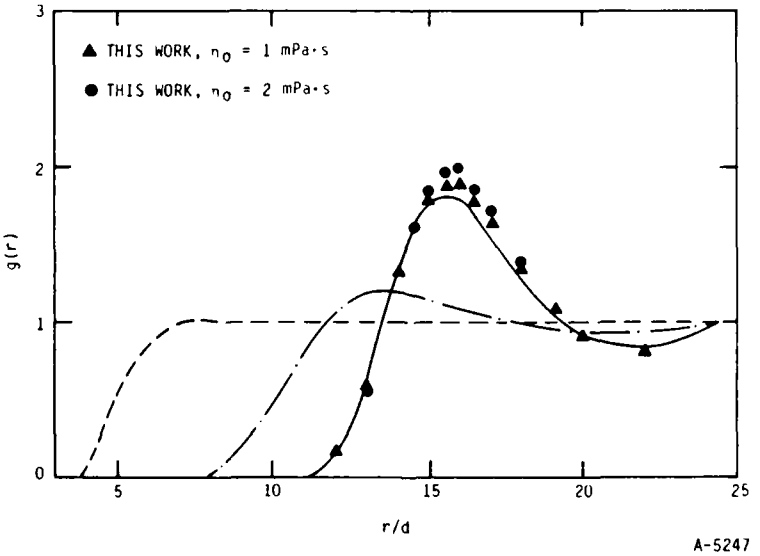

Figure A-2. Radial distribution function as a function of electrolyte concentration when $\phi = 1.5 \times 10^{-4}$; —— n = 10^{-3} mol m^{-3}, —·— n = 10^{-2} mol m^{-3}, ----- n = 10^{-1} mol m^{-3} (after Ref. 42a).

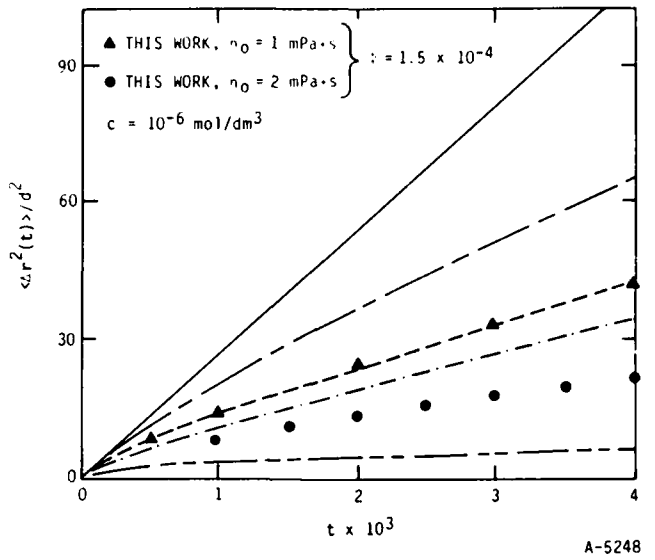

Figure A-3. Mean square displacement as a function of time: ——— free diffusion, — — — ϕ = 5.0 x 10^{-5}, ——— ϕ = 1.5 x 10^{-4}, —·— ϕ = 3.0 x 10^{-4}, —·—·— ϕ = 7.0 x 10^{-4} (after Ref. 42a,43).

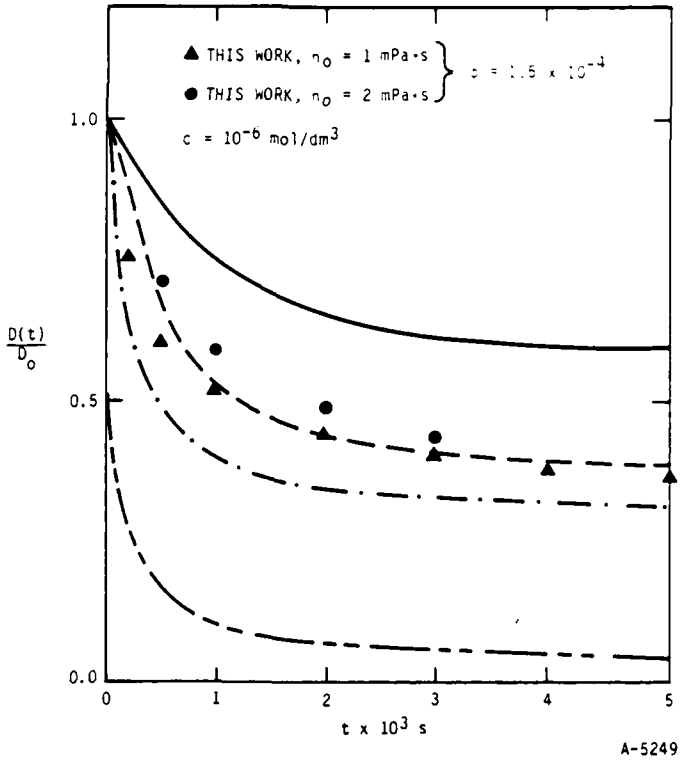

Figure A-4. Time dependence of diffusion coefficient: ——— ϕ = 5.0 x 10^{-5}, ——— ϕ = 1.5 x 10^{-4}, —·— ϕ = 3.0 x 10^{-4}, —·—·— ϕ = 7.0 x 10^{-4} (calculated from $D(t)/D_0 = \langle (r_i(t) - r_i(0))^2 \rangle / 6D_0 t$, not from Eq. (23) (after Ref. 42a).

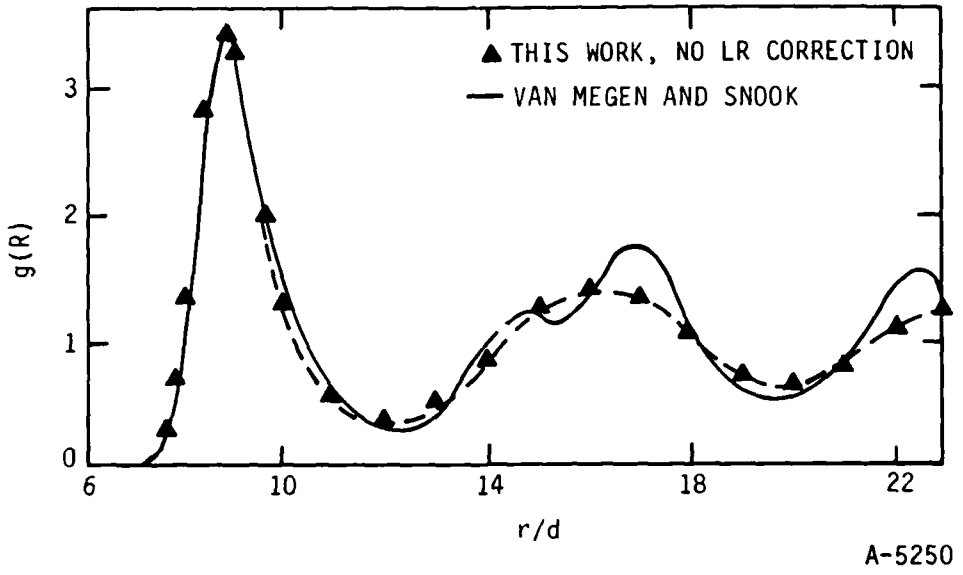

Figure A-5. Radial distribution function for dispersion with $\kappa d = 0.30$ at $\phi = 9.9 \times 10^{-4}$ (after Ref. 29).

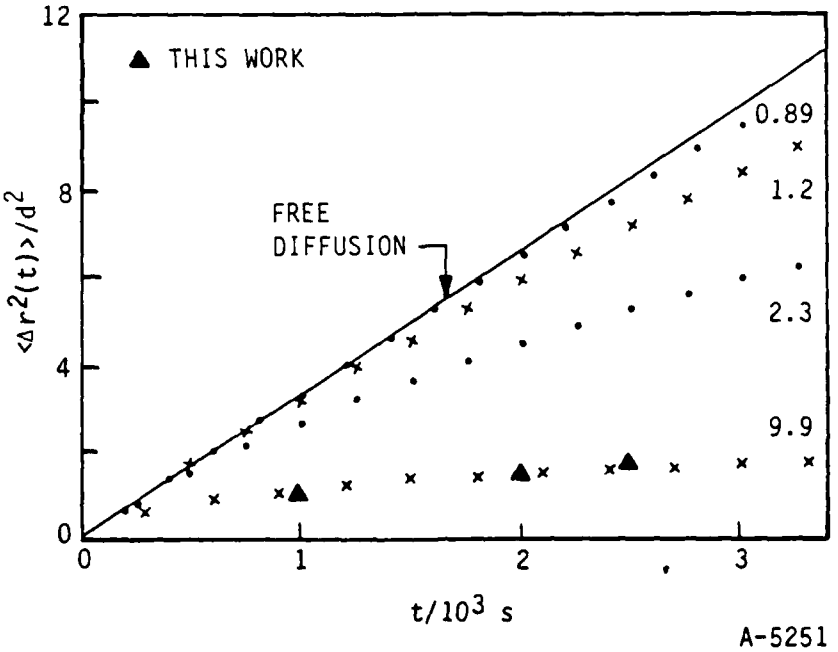

Figure A-6. Mean square displacements for dispersion with $\kappa d = 0.30$ showing free diffusion by the solid line; numbers corresponding to other results represent $\phi \times 10^4$ (after Ref. 29).

because of the slowly changing particle configuration, forces on the particles are correlated, and the average motion is strongly affected.

Our test calculations in Figs. A-2 through A-4 were made for a volume fraction of 1.5×10^{-4} using two different fluid viscosities, 1 and 2 mPa•s. Doubling the usual value of η_o results in halving the single particle diffusion coefficient D_i (cf. Eq. (11)). This significantly retards the average motion of particles in suspension, as can be seen in Figure A-3. In principle, changing η_o should not affect g(r) because it is an equilibrium property solely determined by U. The results in Fig. A-2 approximately bear this out. The discrepancy may be due to using too large a time step Δt in the simulations. Van Megen and Snook[30] have noted that if Δt is too large, peaks in g(r) tend to be artificially flattened. Doubling the viscosity while holding Δt constant effectively halves the time step, and the peak height grows as a consequence. It should be noted that the same Δt reported by Gaylor et al.[42a] was used in these calculations. The remaining discrepancy with their results may be due to running the simulations for an insufficient number of time steps.

In Figs. A-5 and A-6, the results of Van Megen and Snook[29] show the effect of increasing the volume fraction to the value 9.9×10^{-4}. Their results in Fig. A-5 using 256 particles show that the suspension is becoming increasingly ordered with the particles distributed about the sites of a bcc lattice. The strong interactions that promote ordering also greatly inhibit particle motion. This can be seen in Fig. A-6 from the slowly increasing m.s.d. at the highest volume fraction. Our results for g(r) agree well at $r/d<14$, but are poorer for larger values of r. This is probably due to our neglect of long range contributions to the total force from particles beyond the cut-off distance of $\ell/2$. The calculated m.s.d. agrees well probably because its early behavior should be controlled by interactions with particles in the first and second nearest neighbor shells.


DATE
FILMED
28